Highly potent novel multi-armoured IL13Ra2 CAR-T subverts the immunosuppressive microenvironment of Glioblastoma

Maurizio Mangolini[1*], Saket Srivastava[1], Emily Souster[1], Yajing Yang[1], Huimin Wang[1], Rajesh Karattil[1], Liam Schultz[1], Biao Ma[1], Diana Pombal[1], Matthew Greenig[2], Aubin Ramon[2], Pietro Sormanni[2], Shaun Cordoba[1], Shimobi Onuoha[1**]

[1]Chimeris UK, The Works, Unity Campus, London Road, Cambridge, CB22 3EE
[2]Centre for Misfolding Diseases, Yusuf Hamied Department of Chemistry, University of Cambridge, Lensfield road, CB2 1EW Cambridge, UK
*Correspondence: Maurizio.mangolini@chimeris.uk
**Correspondence: Shimobi.Onuoha@chimeris.uk

SUMMARY

Glioblastoma remains one of the most challenging and lethal brain cancers, with limited treatment options. While CAR-T cells have shown promise in some patients, sustaining T-cell activity and overcoming the immunosuppressive tumour microenvironment remain significant hurdles. Here, we present an armoured CAR-T cell design to address these challenges and enhance persistence in GBM tumours. We developed a highly specific humanised single-domain antibody targeting IL13Rα2 and included it alongside four additional modular elements in a single retroviral vector for CAR-T generation. Our results demonstrate that this single-cassette CAR-T cell design possesses high resilience against TGF-β-mediated immunosuppression, enhanced tumour-killing capacity through IL-12 secretion while maintaining a favourable safety profile, extended persistence in the host, and an additional layer of safety control through the incorporation of a suicide switch. Importantly, despite its complexity, the construct can still be manufactured efficiently. These advancements represent a significant step forward in addressing key challenges associated with CAR-T cell therapy in solid tumours.

KEYWORDS

Cell therapy, CAR-T cells, Glioblastoma, IL13Rα2, TGF-β, IL-12, solid tumour, VHH

INTRODUCTION

Glioblastoma (GBM) is one of the most aggressive and lethal forms of brain cancer, with a dismal prognosis despite current standard treatments and the implementation of multimodal treatment strategies. Unfortunately, at present day, the prognosis for glioblastoma remains poor with a median survival of less than 15 months from initial diagnosis, a 2-year survival rate of approximately 26-33% and a 5-year survival rate estimated at just 6.8%[1,2].

In recent years, chimeric antigen receptor (CAR) T cell therapy has emerged as a promising immunotherapeutic approach for treating GBM[3]. Among the various targets explored, interleukin-13 receptor alpha 2 (IL13Rα2) has garnered significant attention as a potential CAR-T cell target for this disease indication. IL13Rα2 is a monomeric high-affinity receptor for interleukin-13 (IL-13) that is overexpressed in most GBM tumours, with studies reporting its presence in 60-75% of cases. Importantly, IL13Rα2 expression is minimal in normal brain tissue, making it an attractive tumour-specific target[4,5,6]. The receptor's overexpression is associated with the mesenchymal GBM subtype and correlates with poor patient survival, further underscoring its relevance as a therapeutic target[7].

CAR-T cells engineered to target IL13Rα2 have shown promising results in preclinical studies triggering a potent anti-tumour immune response. Furthermore, recent clinical trials evaluating IL13Rα2-targeted CAR-T cells in GBM patients have shown encouraging results, with evidence of tumour regression and improved survival in some cases[8,9,10,11]. However, challenges such as limited T-cell persistence and exposure to the immunosuppressive tumor microenvironment (TME) have been observed. One way to overcome the challenges faced by CAR-T cell therapy in treating solid tumours like GBM is to develop "armoured" CAR-T cells with enhanced capabilities.

Similarly to most solid tumours, GBM employs various immune-evasive strategies within their tumour microenvironment (TME) that result in treatment resistance. These mechanisms pose substantial challenges for CAR-T cells, hindering their ability to mount effective antitumor responses and achieve the robust expansion necessary for significant tumour reduction. Among these, the Transforming Growth Factor beta (TGF-β1/TGF-βR2) signalling pathway is particularly significant in promoting T cell dysfunction and limiting their proliferation[12,13,14]. Enhancing CAR-T cells with the ability to produce anti-tumour cytokines is also a promising strategy to overcome the challenges posed by the hostile TME. Interleukin-12 (IL-12) stands out among these cytokines for its remarkable anti-tumour capacity. However, the clinical application of IL-12 has faced significant hurdles due to its potent systemic toxicity[15,16]. Indeed, multiple experimental models and clinical trials have revealed toxicity profiles associated with systemic IL-12 exposure, which has hampered its progression in therapeutic development[17].

Here we show a novel armoured CAR-T cell targeting IL13Rα2, which addresses several key challenges associated with CAR-T cell treatment of GBM. Our approach combines a newly developed, highly specific, humanized single-domain antibody (VHH) against IL13Rα2 with a fourth-generation CAR design that incorporates multiple functional enhancements within a single retroviral vector. This advanced CAR construct includes: -a TGF-β receptor-blocking antibody; - a constitutively active form of the GM-CSF intracellular receptor region; -an engineered single-chain IL-12 sequence; - a modified version of HER2 as a suicide switch for controlled cell elimination. We demonstrate that primary T cells expressing this construct show superior performance compared to conventional CAR-T cells, exhibiting enhanced tumour cell killing, improved proliferation, and prolonged persistence. The blockade of TGF-β signalling significantly enhances the engineered T cells' resistance to immunosuppression, while the attenuated IL-12 activates bystander NK and T cells without observable toxicity. Furthermore, the incorporation of a suicide gene, activated by the FDA-approved drug Trastuzumab

76 emtansine (T-DM1), provides a crucial safety mechanism for the controlled elimination of the
77 engineered cells. *In vitro* and *in vivo* data confirmed the efficacy, survival, and safety profile of
78 these armoured CAR-T cells, even at low doses. Notably, despite the complexity of the
79 construct, we demonstrate manufacturing feasibility in a Good Manufacturing Practices (GMP)
80 - compliant setting. Altogether, our findings offer a promising new avenue for the treatment of
81 GBM and potentially other IL13Rα2-expressing malignancies representing a significant step
82 forward in the field of CAR-T cell therapy for solid tumours.

83 **RESULTS**

84 ***In vitro* screening identifies lead IL13Ra2 VHH for CAR-T cells**

85 The targeting domain of CARs is their most critical component for recognizing and interacting
86 with the desired target antigen. To develop a new CAR targeting IL13Rα2, we created a specific
87 nanobody, due to their advantages in terms of low immunogenicity and small size[18]. The
88 discovery of the IL13Rα2-specific nanobody was achieved through a combination of
89 immunization, phage display, and deep repertoire mining, followed by humanization and
90 functional screening (Figure 1A). In brief, after immunizing alpacas, we generated a phage
91 display library enriched against IL13Rα2, using IL13Rα1 as a deselection target to ensure high
92 specificity for IL13Rα2 while avoiding cross-reactivity with IL13Rα1.

93 Next-generation sequencing (NGS) was then performed on the enriched library, and cluster
94 analysis identified potential binders. The analysis focused on extracting complementarity-
95 determining regions (CDRs) 1, 2, and 3, which were computationally combined to generate
96 artificial sequences for similarity clustering, with the idea that VHHs with similar CDRs should
97 bind the same epitope. Homology groups were formed using a distance matrix that prioritized
98 chemical differences and similarities between amino acids, rather than simpler sequence-
99 identity (Supplementary Figure S1A). The highest frequency sequence from each group was

selected for further characterisation. This approach effectively sampled the diversity of the screened library and reduced the risk of clonal dominance.

Parallel to NGS analysis, traditional panning and clone selection by colony picking were also performed, yielding complementary insights. A total of 50 clusters were initially identified, with 20 clusters progressing to production and subsequent functional evaluation (Figure 1B,C). Binding specificity assays identified eight molecules that bound IL13Rα2 without cross-reactivity to IL13Rα1. However, despite the extensive diversity of the library, repeated rounds of panning narrowed the functional binders to two primary sequences. This observation suggests a potential bias in phage display selection that was not mirrored in the broader diversity identified through NGS.

Half maximal effective concentration (EC_{50}) and thermal stability (T_m) analysis revealed that the majority of the selected binders exhibited favourable melting temperatures, indicative of robust biophysical properties in addition to specific binding (Figures 1D,E). Based on these combined biophysical and functional analyses, clone C1.1 from cluster 1 emerged as the lead candidate for incorporation into the IL13Rα2 CAR, designated IL13Ra2 c1.1.

We then performed humanisation of the Clone c1.1 using the AbNatiV VHH humanisation pipeline, as reported in Ramon et al. [19]. This AI-based approach samples humanising mutations ensuring retention of binding affinity and favourable VHH biophysical properties (Figure 1F). The humanized variants $c1.1^{en}$ and $c1.1^{ex}$, respectively from the enhanced and exhaustive AbNatiV humanisation pipelines[19] showed equivalent stability and specificity compared to the wild-type counterpart. To further assess the specificity of these VHHs for IL13Rα2 and minimize the risk of off-target binding effects, we conducted an extensive cross-reactivity study. This study evaluated the binding of the VHHs against approximately 6,000 native human membrane proteins. Remarkably, all three clones demonstrated minimal cross-reactivity with

124 other proteins. Among them, c1.1^{en} exhibited the strongest specific binding to IL13Rα2
125 (Supplementary Figure S1B).
126 Clones c1.1, c1.1^{en} and c1.1^{ex} were then inserted into a retroviral vector encoding a CAR
127 construct with CD28 and CD3ζ intracellular signalling domains (Figure 1G). These were tested
128 against the T98G glioma cell line (IL13Rα2-negative) and SUPT1 cells engineered to express
129 IL13Rα1 to assess off-target and cross-reactivity. Notably, the humanized variant c1.1^{en}
130 exhibited minimal off-target activity against IL13Rα1, corroborating its specificity and reduced
131 background activity or "tonic signalling" compared to both the wild-type llama-derived CAR
132 and the exhaustive-humanized c1.1^{ex} CAR while retaining high cytolytic activity against
133 IL13Rα2-expressing glioma cell lines and SUPT1-IL13Rα2 cells (Figure 1H,I and
134 Supplementary Figure S1C-G). This reduction in background activity is likely due to improved
135 biophysical properties, such as increased solubility and thermal stability, engineered during the
136 humanization process. Further validation was conducted using CellTrace Violet (CTV)
137 proliferation assays on IL13Rα2-positive and IL13Rα2-negative SupT1 cells (Figure 1J).
138 These results highlight the advantages of the engineered humanized clone C1.1^{en},
139 demonstrating its suitability for clinical development and its potential to mitigate adverse
140 effects associated with CAR tonic signalling.

141 **dsFvTBRII/CCR overcomes the inhibitory effects of TGF-b and induces CAR-T cell**
142 **persistence**

143 TME-induced T cell inhibition and reduced persistence are among the major factors limiting
144 the efficacy of CAR-T cells in solid tumours[20]. TGF-β, abundantly secreted by tumor and
145 stromal cells in glioblastoma, potently suppresses CAR-T proliferation, drives exhaustion, and
146 fosters an immunosuppressive microenvironment, thereby limiting therapeutic efficacy[21,22,23].
147 To overcome these limitations, we designed a fusion protein containing two key elements: an
148 extracellular region consisting of a blocking antibody for the TGF-β receptor II (TBRII) and

149 the transmembrane and truncated intracellular domains of the granulocyte-macrophage colony-
150 stimulating factor (GM-CSF) receptor as a chimeric costimulatory receptor (CCR) (Figure 2A).
151 This innovative architecture leverages the disulfide bond of the TBRII antibody region to
152 achieve constitutive downstream activity of the receptor. We first validated the blocking
153 functionality of the disulfide-stabilized single-chain variable fragment (dsFv) antibody derived
154 from the original Fab sequence. Using a reporter cell line that quantifies TGF-β response
155 through secreted embryonic alkaline phosphatase (SEAP) production, we demonstrated that
156 the dsFv antibody retained the TGF-β blocking capacity of the original Fab version (Figure
157 2B). Subsequently, we evaluated the function of the intracellular component. We generated two
158 single cassette constructs expressing the dsFvTBRII region fused with different orientations of
159 the GM-CSF receptor chains: alpha-beta and beta-alpha. The overexpression of these
160 constructs in Jurkat cells revealed that the beta-alpha orientation was more potent in activating
161 STAT5 (Figure 2C). This finding was further corroborated using GM-CSF reporter cell lines
162 (Supplementary Figure 2A). Moreover, we confirmed that the final chimeric receptor design
163 (dsFvTBRII/CCR) maintained its TGF-β blocking functionality when tested using TGF-β
164 reporter cells (Figure 2D). To assess whether the dsFvTBRII/CCR module would enhance
165 CAR-T cell resistance to TGF-β and improve their persistence, we integrated this construct into
166 the IL13Rα2 c1.1^{en} CAR design, separating the two components with a T2A self-cleaving
167 peptide. Comparative analysis revealed that CAR-T cells incorporating the dsFvTBRII/CCR
168 module exhibited reduced susceptibility to TGF-β pathway activation, measured by decreased
169 SMAD2/3 phosphorylation (Figure 2E and Supplementary Figure S2B). Furthermore, in
170 cytokine-deprived *in vitro* culture conditions (Figure 2F), control cells incurred complete cell
171 death within 10 days, whereas cells overexpressing the CCR maintained viability for up to 40
172 days (Figure 2G). To determine whether the extended viability observed in CAR-T cells
173 expressing the CCR module was accompanied by enhanced proliferative capacity, we

174 conducted a dye dilution assay to track cell division over 7 days. Our results demonstrated that
175 CAR-T cells incorporating the CCR module underwent multiple rounds of proliferation,
176 significantly outperforming the control cells (Figure 2H). This finding was further corroborated
177 by the rapid increase in the proportion of CCR-expressing CAR-T cells within the total cell
178 population over time (Figure 2I). The long-term cytotoxic function and proliferative capacity
179 of CAR-T cells were assessed in vitro over 7 weeks, with additional glioma tumor target cells
180 added weekly to the co-culture. The CCR-expressing CAR-T cells maintained full cytolytic
181 activity for at least 5 weeks, compared to only 3 weeks for non-armored CAR-T cells
182 (Supplementary Figure S2C). To further validate the efficacy of our dsFvTBRII/CCR module,
183 we employed the well-characterized CD19 CAR-T cell model as an additional experimental
184 system. *In vitro* experiments demonstrated that overexpression of the dsFvTBRII/CCR
185 construct in CD19 CAR-T cells conferred partial protection against the cytotoxic inhibitory
186 effects of TGF-β (Supplementary Figure S2D). Moreover, we observed that cells incorporating
187 this additional module displayed extended longevity compared to those expressing only the
188 CAR construct, suggesting that the ability of the dsFvTBRII/CCR to enhance CAR-T cells'
189 persistence is independent of the upstream CAR architecture (Supplementary Figure S2E,F).
190 Collectively, these results indicate that the incorporation of the dsFvTBRII/CCR module
191 confers enhanced resistance to TGF-β-mediated immunosuppression and significantly extends
192 the survival and the proliferative potential of CAR-T cells in the absence of exogenous cytokine
193 support, potentially overcoming some of the challenges of the tumour microenvironment.

194 **Development of a scIL12 with an improved safety profile**

195 IL-12 is a potent pro-inflammatory cytokine that is crucial in bridging innate and adaptive
196 immunity. It has several beneficial effects in the context of cancer immunotherapy, such as
197 enhancing T cell proliferation and cytotoxicity, activating and recruiting NK cells and NKT
198 cells and stimulating interferon-gamma (IFNγ) production[24]. However, its potent anti-tumour

199 effects are concomitant with severe toxicities in clinical trials, limiting its therapeutic
200 application[17]. To mitigate potential toxicity, we compared different single-chain IL-12 (scIL12)
201 constructs. We focused on two primary configurations that have previously shown different
202 biological activities[25]: One comprising the p40 subunit followed by the p35 subunit ($scIL12^{wt}$),
203 and another with the reverse arrangement p35 followed by p40 ($scIL12^{inv}$). Additionally, we
204 examined the canonical G_4S linker using different amino acid length compositions connecting
205 these subunits. This aspect was motivated by the understanding that linker length can
206 significantly influence protein flexibility[26], potentially affecting the biological activity and
207 safety profile of the scIL12 forms. To evaluate the functional differences among the various
208 scIL12s, we assessed their capacity to activate IL-12 signalling using a commercially available
209 IL-12 reporter cell line stimulated with scIL12 purified proteins. This system allows
210 quantifying the activation of IL-12 signalling, measuring the production of SEAP following
211 IL-12 binding and the subsequent activation of STAT4 (Figure 3A). The results showed that
212 the scIL12 proteins with the p35-linker-p40 subunit configuration exhibited reduced activity
213 compared to the p40-linker-p35 arrangement. Furthermore, shortening the linker length from
214 15 to 7 amino acids in the p35-linker-p40 construct resulted in an additional decrease in
215 functional activity (Figure 3B). Notably, this difference was evident only in the p35-p40
216 orientation. Further investigation of the linker length in the inverted orientation revealed no
217 correlation between shorter linker lengths and signal downregulation. Indeed, the maximum
218 reduction in signalling was achieved using a 7-amino acid linker, suggesting that this specific
219 length optimally decreases the biological activity of the inverted IL-12 construct
220 (Supplementary Figure S3A).
221 Activation of the IL-12 signalling is mediated by initial ligation of the p40 subunit to the IL-
222 12Rβ1 and subsequent heterodimerisation with IL-12Rβ2 mediated by the p35 subunit[27,28]. To
223 investigate the impact of linker length and subunit order on the structural integrity and receptor

224 binding affinity of our engineered scIL12 variants, we conducted an ELISA-based binding
225 assay. Our results revealed that the orientation of the IL-12 subunits significantly influenced
226 receptor binding. Specifically, scIL12 constructs with the p35-p40 orientation demonstrated
227 reduced binding affinity to IL-12Rβ1 compared to those with the p40-p35 orientation (Figure
228 3C). Interestingly, we observed no significant differences in binding affinity to IL-12Rβ2
229 across the various scIL12 orientations (Supplementary Figure S3B). This indicates that the
230 order and spatial arrangement of the subunits play a crucial role in maintaining the proper
231 conformation for receptor interaction. To further evaluate the biological activity of our
232 engineered scIL12, we tested their efficacy on T cells and NK cells. The results showed that
233 STAT4 phosphorylation (pSTAT4) levels varied in a specific manner, influenced by the length
234 of the linker connecting the IL-12 subunits and their orientation (Figure 3D,E). To validate the
235 functionality of scIL12 in the context of CAR-T cells, we incorporated scIL12^{wt} (p40-15aa-
236 p35) or scIL12^{inv} (p35-7aa-p40) in the IL13Rα2 c1.1^{en} CAR vector. Engineered cells were co-
237 cultured using cell-permeable supports with primary isolated T and NK cells for 72 hours to
238 assess IL-12-mediated activation through intracellular staining of pSTAT4 and measurement
239 of IFNg production (Figure 3F). Our results demonstrated that while the IL13Rα2 c1.1^{en} +
240 scIL12^{inv} construct maintained the capacity to activate both T and NK cells, its potency was
241 notably reduced compared to the scIL12^{wt} cells (Figure 3G,H). The enhanced safety profile
242 was particularly evident in the reduced production of IFNγ, the cytokine primarily responsible
243 for IL-12 toxicity, by NK cells following IL-12 stimulation (Supplementary Figure S3C). Some
244 studies demonstrate antigen-dependent regulation of IL-12 secretion in armored CAR-T cells[29].
245 To determine if this occurs with our specific construct, we evaluated scIL-12 expression in both
246 wild-type and inverted configurations upon antigen stimulation. Results revealed a trend
247 toward increased IL-12 secretion, potentially due to CAR-T activation driving enhanced
248 proliferation and thus a greater number of IL-12-producing cells (Supplementary Figure S3D).

249 To assess both the anti-tumour efficacy and potential toxicity of our engineered scIL12 *in vivo*,
250 we utilized an aggressive mouse melanoma model using B16.F10 cells transduced to express
251 GD2. We established tumours in syngeneic mice by injecting B16.F10-GD2 cells and allowing
252 them to engraft for 8 days. Subsequently, we administered a single intravenous dose of 2.5 ×
253 10^6 GD2, GD2-mIL12^{WT}, or GD2-mIL12^{inv} CAR-T cells (Figure 3I). Our results demonstrated
254 that while GD2 CAR-T cells alone provided limited tumour control, both IL-12-expressing
255 CAR-T cell groups showed remarkable anti-tumour efficacy, with tumours remaining nearly
256 undetectable (Figure 3J and Supplementary Figure S3E). Notably, we observed a complete
257 contrast in toxicity profiles between the two IL-12 variants. Mice receiving GD2-mIL12^{wt}
258 CAR-T cells experienced significant weight loss, while mice treated with GD2-mIL12^{inv} CAR-
259 T cells maintained stable body weight, suggesting a substantially improved safety profile of
260 IL12^{inv} (Figure 3K).
261 In conclusion, our findings demonstrate that the engineered scIL12 with inverted subunit
262 orientation (p35-p40) and shortened linker length maintains a significant level of biological
263 activity while substantially reducing the systemic toxicity commonly associated with IL-12
264 therapy.

265 **HER2 as a safety switch and CAR-T detection marker**

266 To address potential safety concerns associated with IL-12 secretion, induced enhanced
267 proliferation and prolonged persistence of our CAR-T cells, we incorporated an elimination
268 switch into our construct. This safety mechanism is designed to provide a means of controlling
269 the engineered T cells *in vivo* if required[30]. For this purpose, we selected HER2 as the protein
270 of interest due to its compatibility with an existing FDA-approved targeted therapy.
271 Trastuzumab emtansine (T-DM1), an antibody-drug conjugate targeting HER2, has
272 demonstrated high efficacy and is generally well-tolerated in clinical settings[31]. In our efforts
273 to optimise the HER2-based suicide switch module, we explored various modifications to

274 enhance its efficacy while reducing its overall length in our construct (Figure 4A). Firstly, we
275 replaced the native HER2 transmembrane domain with that of CD5, a protein known to
276 facilitate rapid receptor internalisation in T cells[32]. Our results showed that cells expressing the
277 HER2-CD5 transmembrane construct exhibited significantly increased sensitivity to T-DM1
278 compared to those expressing the original HER2 construct. We further optimized the suicide
279 switch by focusing on its extracellular region. We generated a truncated version of the HER2
280 extracellular domain, retaining only the specific region containing the docking site for T-DM1
281 (DHER2^{CD5}). This modification was designed to minimize the size of the construct while
282 preserving its essential function as a safety switch. Our results demonstrated that this truncation
283 did not compromise the construct's sensitivity to T-DM1. Remarkably, we observed an increase
284 in sensitivity to the antibody-drug conjugate compared to the full-length extracellular domain
285 (Figure 4B). To further validate our findings, we extended our investigation to primary T cells,
286 comparing the efficacy of T-DM1-mediated elimination between cells expressing the IL13Rα2
287 c1.1^{en}-DHER2^{CD5} CAR construct and those expressing the CAR alone. T cells engineered with
288 the IL13Rα2 c1.1^{en}-DHER2^{CD5} CAR construct exhibited significant susceptibility to T-DM1-
289 induced elimination, whereas those expressing only the CAR remained largely unaffected
290 (Figure 4C,D). We also observed a notable decrease in CAR expression intensity, suggesting
291 that T-DM1 preferentially affects cells with higher CAR expression levels. This observation
292 indicates that the reduction of highly expressing cells, which are likely responsible for
293 increased toxicity, occurs first (Figure 4E). These findings support the translational potential
294 of our optimized suicide switch strategy for clinical applications.

295 **Generation and validation of IL13Rα2 c1.1^{en} multi-armoured CAR**

296 Our findings demonstrate that each individual armoured module functions effectively within
297 the context of the IL13Rα2 c1.1^{en} CAR construct. However, combining all modules into a
298 single transgene cassette poses a significant challenge due to size constraints. Viral delivery

299 systems are typically limited to payloads of approximately 8-9kb, and larger constructs result
300 in diminished expression efficiency that correlates with their increased size[33]. To address this
301 limitation and maximise transduction efficiency, we developed an optimised two-step viral
302 production protocol. This approach involves creating an intermediate viral producer cell line
303 pseudotyped with the vesicular stomatitis virus envelope (VSV-G). This intermediate line is
304 then used to establish a stable viral producer cell line that generates viruses incorporating the
305 RD114 envelope protein, which has been shown to have superior transduction ability in
306 primary human lymphocytes[34,35] (Supplementary Figure S4A). We then tested this protocol
307 using IL13Rα2 c1.1^{en} Arm CAR, a bicistronic γ-retroviral vector encoding IL13Rα2 c1.1^{en},
308 DHER2^{CD5}, dsFvTBRII/CCR and IL12^{inv} all separated by a self-cleaving 2A peptide and
309 transcribed from a single promoter (Supplementary Figure S4B). Upon transduction of
310 autologous T cells with this construct, we observed remarkably efficient expression of each
311 individual component. Notably, and unexpectedly, all components were expressed at a near-
312 perfect 1:1 ratio throughout the entire construct (Supplementary Figure S4B). Testing the
313 IL13Rα2 c1.1^{en} Arm CAR and IL13Rα2 c1.1^{en} CAR using GBM cell lines revealed that the
314 armoured CAR demonstrated superior cytotoxic activity compared to the CAR alone and single
315 armoured CARs (Figure 5A and Supplementary Figure S4D). Notably, we detected
316 significantly higher levels of IFNγ production in the IL13Rα2 c1.1^{en} Arm cells, suggesting that
317 the IL12^{inv} component remained functional (Supplementary Figure S4E). We confirmed this
318 by measuring NK cell pSTAT4 levels, which showed that IL-12 was indeed present and
319 functional (Supplementary Figure S4F).
320 T cell exhaustion poses a major obstacle to long-term CAR-T efficacy, marked by
321 dysfunctional states with reduced proliferation, impaired anti-tumor functions, and co-
322 upregulation of inhibitory receptors like TIM3, LAG3, and PD-1[36]. We therefore assessed these
323 markers via co-expression profiles in transduced cells. After 3-day co-culture with IL13Rα2-

324 expressing targets, TIM3/LAG3/PD-1 expression was evaluated on IL13Rα2 c1.1^{en} and
325 IL13Rα2 c1.1^{en} Arm CAR T cells. In CD4^{+} and CD8^{+} subsets, stimulated CAR T cells showed
326 elevated exhaustion markers versus NT cells; most were double-positive, with triple-positive
327 (TIM3^{+}LAG3^{+}PD-1^{+}) cells limited. Distributions were comparable between IL13Rα2 c1.1^{en}
328 and Arm CAR T cells, indicating our armored elements do not promote terminal exhaustion
329 (Figure 5B).
330 To evaluate the enhanced capabilities of the IL13Rα2 c1.1^{en} Arm compared to the standard
331 IL13Rα2 c1.1^{en} CAR, we conducted a comprehensive series of stress tests (Figure 5C). Our
332 initial assessment focused on the advantages conferred by the CCR module under cytokine-
333 deprived conditions. Transduced autologous T cells were cultured without cytokines for 96
334 hours, after which we measured their killing activity against SupT1 IL13Rα2 target cells. The
335 results clearly demonstrated that IL13Rα2 c1.1^{en} Arm-modified T cells exhibited superior
336 expansion, survival, and target cell elimination efficacy in this nutrient-deprived environment
337 compared to their standard CAR counterparts (Figure 5D). We then examined the cells' killing
338 capacity following antigen stimulation in the presence of TGF-β by culturing CAR-T cells on
339 plates coated with IL13Ra2 protein and TGF-β for 96 hours before assessing their cytotoxic
340 activity. The IL13Rα2 c1.1^{en} Arm consistently outperformed the IL13Rα2 c1.1^{en} CAR under
341 these conditions (Figure 5E). To test the regulatory capability of the HER2 module, we cultured
342 the cells in the presence or absence of T-DM1. Following T-DM1 exposure, the cells lost their
343 ability to kill target cells and secrete IFNγ, demonstrating effective regulation through the
344 safety switch (Figure 5F and Supplementary Figure S4G). To further assess the superior
345 performance of the IL13Rα2 c1.1^{en} Arm CAR, we conducted a stress test using SNB19
346 glioblastoma cells. CAR-T cells were co-cultured with SNB19 cells for 7 days, then transferred
347 to freshly plated SNB19 cells for an additional 7 days. Following this extended challenge,
348 CAR-T cells were normalized and co-cultured with SUPT1-IL13Rα2 cells to measure their

349 killing activity (Figure 5G). The results demonstrated that the IL13Rα2 c1.1^{en} Arm
350 significantly outperformed the IL13Rα2 c1.1^{en} CAR, even after prolonged exposure to tumour
351 cells (Figure 5H,I). These comprehensive tests highlight the advantages of our armoured CAR
352 design, demonstrating improved persistence, killing efficiency, and maintained functionality
353 under various challenging conditions that mimic the hostile tumour microenvironment. To
354 further evaluate the IL13Rα2 c1.1^{en} Arm CAR-T cells in a more physiologically relevant
355 manner, we used a well characterised GBM tumour model by orthotopically injecting U87
356 cells, modified to stably overexpress IL13Rα2, in immunodeficient mice[37]. Following 8 days
357 of engraftment, mice were grouped based on similar bioluminescence signals and intracranially
358 injected with $6.25*10^4$ CAR-T cells (Figure 6A). Remarkably, while IL13Rα2 c1.1^{en} CAR-T
359 cells failed to eradicate tumors in 3 out of 5 mice, complete tumour eradication was achieved
360 in all 5 mice treated with IL13Rα2 c1.1^{en} Arm CAR-T cells (Figure 6B,C). Importantly, the
361 body weight of the animals remained stable throughout the study, underlining the safety profile
362 of our CAR-T construct (Figure 6D). We also assessed IL13Rα2 c1.1^{en} Arm CAR-T cells safety
363 and efficacy in a subcutaneous U87-IL13Rα2 xenograft model. Tumors reaching 200 mm^3
364 were treated with intravenous CAR-T cells; after 30 days, IL13Rα2 c1.1^{en} Arm CAR-T
365 outperform non-armored controls, with persistent circulating IL13Rα2 c1.1^{en} Arm CAR-T cells
366 detectable by FACS (non-armored undetectable) (Figure 6E,J). Sustained tumor control was
367 also observed at lower CAR-T doses (Supplementary Figure 5A). To evaluate safety, peripheral
368 IFN-γ was measured in blood from treated animals. Animals receiving IL13Rα2 c1.1^{en} Arm
369 CAR-T cells showed higher IFN-γ levels than those treated with IL13Rα2 c1.1^{en} CAR-T alone,
370 where IFN-γ was undetectable, aligning with limited CAR-T detection and higher tumor
371 burdens in the latter (Figure 6K and Supplementary Figure 5B). Notably, despite detectable
372 IFN-γ in the IL13Rα2 c1.1^{en} Arm cohort, no overt systemic toxicity occurred, as body weights
373 remained comparable to CAR-alone and NT controls without decline. These findings

374 collectively highlight the superior anti-tumour efficacy of our IL13Rα2 c1.1^{en} Arm CAR-T
375 cells in a clinically relevant GBM model, while also demonstrating the potential for precise
376 control of CAR-T cell activity to enhance safety.

377 **Validation of the IL13Rα2 c1.1^{en} multi-armoured CAR for clinical purpose**

378 Given the complexity of our CAR-T construct, we aimed to evaluate the feasibility of
379 manufacturing IL13Rα2 c1.1^{en} Arm CAR-T cells within a Good Manufacturing Practice
380 (GMP) workflow. We activated sorted CD3^{+} T cells from two healthy donors using T Cell
381 TransAct™. Forty-eight hours later, these cells were transduced with clinical-grade IL13Rα2
382 c1.1^{en} Arm viral supernatant (titer 4.89x10^{8} TU/ml) at varying multiplicities of infection (MOI).
383 The cells were then cultured using the G-Rex cell culture platform, which utilises gas-
384 permeable membrane technology to enhance oxygen delivery and nutrient exchange[38], in the
385 presence of IL7/IL15 and an optimized serum-free cell culture medium (Figure 7A). Notably,
386 we observed a dose-dependent transduction efficiency, achieving a good level of CAR
387 expression (>20%) even at the lowest MOI tested, with peak expression occurring five days
388 post-transduction (Figure 7B). According to current FDA recommendations, the maximum
389 allowable vector copy number (VCN) is five copies per transduced cell for virally transduced
390 cell therapy products[39]. Our analysis of VCN seven days post-transduction confirmed that this
391 limit was not exceeded by any of the MOIs tested, demonstrating the construct's compatibility
392 with GMP standards and regulatory guidelines (Figure 7C). The expansion and propagation of
393 the cells were monitored for up to 10 days following T cell isolation. Results showed a
394 significant increase in cell numbers, with up to 30-fold expansion and an average total T cell
395 count reaching 10^{9} cells (Figure 7D). Further analysis of T cell subsets revealed a shift in the
396 composition over time. There was a progressive decrease in T memory stem (Tscm) cells,
397 accompanied by an increase in effector memory T cells (Tem cells). Interestingly, the
398 percentage of central memory (Tcm) cells, a population with self-renewal capability, better

399 persistence and antitumor immunity[40], remained stable throughout the expansion period
400 (Figure 7E). On the final day of manufacturing (day 10), the CD4/CD8 ratio was approximately
401 1:4 (Figure 7F). The cells exhibited expression of Lag3 and Tim3, with low expression of PD1
402 (Figure 7G). To validate the functionality of our CAR-T cells at the end of the manufacturing
403 process, we assessed their ability to kill target cells. The data demonstrated that the cells
404 maintained significant killing activity even after the 10-day manufacturing period (Figure 7H).
405 Together, these data demonstrate that IL13Rα2 c1.1^{en} Arm CAR-T cells can be manufactured
406 using a GMP adaptable process while retaining their cytotoxic capabilities, suggesting their
407 potential effectiveness in targeting cancer cells upon administration.

408 **DISCUSSION**

409 Recent clinical studies have demonstrated promising results for CAR-T cell therapy in GBM
410 patients. However, the efficacy of this approach has been constrained by limited CAR-T cell
411 persistence and the immunosuppressive nature of the TME. To address these challenges, we
412 describe here a novel, multi-functional CAR-T construct within a single cassette.

413 IL13Rα2 represents an exciting molecular target for cell therapy, primarily due to its specific
414 expression in GBM and its presence in cancer stem cells. Most current efforts, including
415 clinical trials, have utilised the IL13 binder known as Zetakine to target IL13Rα2. However, a
416 significant challenge with using IL-13 Zetakine is its lack of selectivity, as it also binds to
417 IL13Rα1. To address this cross-reactivity, researchers have developed a mutated form (E13Y)
418 for CAR-T cell preparation, although this approach has shown limited efficacy. Subsequent
419 enhancements included the incorporation of different co-stimulatory molecules that increased
420 efficacy[41,42,43,44]. These findings have undoubtedly contributed to the advancement of IL13Rα2
421 cell therapies for GBM. Our studies corroborated these conclusions while also revealing a
422 novel high-throughput approach to identify new binders for IL13Rα2-targeted therapy.

423 Through a humanization process, we successfully identified a new enhanced IL13Rα2 binder
424 that demonstrates high specificity for IL13Rα2. The approach enabled the generation of a
425 highly tractable single-domain antibody with enhanced selectivity for IL13Rα2, reduced
426 immunogenicity, and excellent biophysical properties, making it more suitable for development
427 as a CAR targeting domain for the treatment of GBM.

428 Two recent clinical studies involving patients with recurrent glioblastoma treated with locally
429 infused CAR-T cells demonstrated tumour reductions in nearly all participants, with substantial
430 regressions observed within 24-48 hours post-infusion. However, the majority of these
431 responses proved to be transient, with tumour recurrence noted in subsequent follow-ups[45,10].
432 One proposed solution to this challenge is the administration of repeated doses of CAR-T cells.
433 While this approach has been shown to be safe in a cohort of 65 patients, it presents significant
434 limitations in terms of feasibility, primarily due to the complexities and costs associated with
435 cell manufacturing[11]. To address these limitations, we opted for an alternative strategy focused
436 on enhancing the CAR-T cells' ability to secrete or express factors that can counteract the
437 immunosuppressive nature of the tumour microenvironment. Indeed, we focused our attention
438 on two key factors: TGF-β and IL-12.

439 TGF-β is known to induce Treg-like cell conversion and PD-1-dependent T cell exhaustion,
440 significantly inhibiting the proliferation and activity of CAR-T cells both *in vitro* and *in*
441 *vivo*[46,47,14]. To counteract this effect, we developed a novel disulfide-stabilized Fv antibody
442 targeting TGF-β receptor II, capable of blocking the downstream activation of TGF-β
443 signalling. We further innovated by coupling this antibody with the α and β chains of the GM-
444 CSF receptor to generate a constitutive active intracellular signal, leveraging the disulfide bond
445 for this purpose. The expression of this combined module led to remarkable results, with cells
446 persisting *in vitro* for over a month. These engineered cells demonstrated the ability to undergo

447 multiple rounds of expansion while maintaining impressive *in vitro* cytotoxicity even after
448 TGF-β treatment. Notably, our experiments revealed that the β/α orientation of the GM-CSF
449 receptor chains produced a more intense signal compared to the α/β configuration, as evidenced
450 by enhanced STAT5 activation. This finding suggests that our module not only offers the
451 advantage of being cytokine or stimulus-independent compared to other approaches[48], but also
452 allows for modulation based on CAR architecture or when a more dampened STAT5
453 intracellular activation is desired. While the enhanced proliferation capacity of these cells could
454 potentially lead to concerns about lymphoproliferative syndromes, our in vitro data suggest
455 that the presence of the GM-CSF CCR alone is not sufficient to cause such complications, as
456 the cells eventually undergo natural cell death. Notably, a similar approach using a signalling
457 cytokine receptor that triggers the IL-7 signalling axis (C7R) has been recently shown to be
458 well-tolerated in young patients with CNS tumours[49,50]. This suggests a low risk for adverse
459 events if our CAR T-cell and CCR combination strategy were to be employed for GBM
460 treatment.

461 IL-12 is a crucial cytokine that plays a significant role in the regulation of immune responses
462 by mainly enhancing the cytotoxic activity of NK and T cells through increased production of
463 IFNγ[51,52]. Given its powerful antitumor function, there has been considerable interest in using
464 IL-12 as an adjuvant in cell therapy and immunotherapy[53]. However, due to its potency being
465 coupled with high toxicity, recent efforts to develop more tolerable versions of the cytokine
466 have been explored. Attempts to regulate the expression of a secretable IL-12 under an
467 inducible NFAT promoter in adoptively transferred T-cell therapy still resulted in unwanted
468 toxicities due to the systemic distribution of the cytokine or a partial leakage of the NFAT gene
469 regulation system[54]. To address this issue, many research groups have explored membrane-
470 bound or -tethered approaches, sometimes coupled with locoregional delivery of CAR-T cells,
471 to limit IL-12 distribution[55,56,57]. While these strategies have demonstrated improved safety

472 profiles, they may potentially limit the full anticancer potential of IL-12 by restricting its ability
473 to activate other cell types. To avoid these limitations, we pursued a different approach to
474 harness the benefits of IL-12 while mitigating its systemic toxicity. Indeed, we leveraged the
475 heterodimeric nature of the IL-12 protein, which is composed of p35 and p40 subunits that
476 together form the biologically active IL-12p70. We created a single-chain form that expresses
477 the p35 subunit in front of the p40 ($IL12^{inv}$), a configuration known to reduce the protein's
478 biological activity. Through experimentation with various linker lengths separating the two
479 subunits, we discovered that a 7-amino acid linker most effectively decreased the biological
480 activity of the construct. Our data suggest that this reduction is primarily due to a lower affinity
481 for the IL-12Rb1 receptor. While a more comprehensive analysis is needed, our current
482 interpretation is that inverting the two subunits either inhibits the correct folding of the protein
483 or causes the p35 subunit to mask the p40 region responsible for receptor binding.
484 Nevertheless, given that p40 binding to the receptor is the initial and limiting step in IL-12
485 signalling[27], our inverted scIL12 exhibits significantly reduced activation potency. This novel
486 approach results in a protein that still retains all the IL-12's beneficial properties but with a
487 much lower risk of systemic toxicity. In conclusion, by fine-tuning the structure and activity of
488 IL-12, we created a safer version of this potent cytokine for use in cancer immunotherapy,
489 potentially overcoming the limitations of previous strategies while maintaining its broad
490 immunostimulatory effects.

491 CAR-T therapy is generally considered safe, but severe side effects such as cytokine release
492 syndrome (CRS) and immune effector cell-associated neurotoxicity syndrome (ICANS),
493 though rare, can still occur. To address these risks, safety switches have become a crucial
494 component in cell therapy development, offering a mechanism to control or eliminate
495 engineered cells in case of severe toxicities. While various approaches are being explored, the
496 most common strategies aim to eliminate CAR-T cells entirely. Among these approaches, the

497 inducible caspase-9 suicide gene system (iCas9), ganciclovir-activated switches, and antibody-
498 dependent cell-mediated cytotoxicity (ADCC) switches are the most frequently utilised. The
499 iCas9 method has shown promising results in clinical trials[58,59], but its clinical application is
500 limited by the lack of regulatory approval for its inducer drugs (AP1903 or AP20187) in cell
501 therapy. Ganciclovir-activated switches, derived from non-human sequences, pose potential
502 immunogenicity risks, potentially inducing both humoral and cellular immune responses
503 against CAR-T cells. Given these limitations, we focused our efforts on developing an ADCC
504 switch. We engineered a truncated version of HER2, retaining only domain IV, which binds to
505 T-DM1, a safe and commercially available drug. Additionally, to enhance the internalisation
506 efficiency of the drug, we replaced the HER2 transmembrane domain with that of CD5. Our
507 preliminary results demonstrate almost complete clearance of CAR-T cells within 48 hours *in*
508 *vitro*. Furthermore, this T-DM1-based switch is compatible with established GBM delivery
509 routes like Ommaya reservoirs or intra-arterial infusion, which bypass the blood-brain barrier
510 for targeted intracranial drug access without systemic toxicity. The efficacy of our approach,
511 achieving approximately 85% elimination, is comparable to clinically used iCasp9-based
512 strategies[60]. This offers a potentially safer and more clinically applicable method for controlling
513 CAR-T cell activity, addressing key challenges in current safety switch technologies.

514 In conclusion, our research represents a promising advancement in CAR T-cell therapy. Despite
515 recent encouraging outcomes, CAR-T cell therapy for solid tumours remains a significant
516 challenge, primarily due to the transient nature of treatment responses observed in many
517 clinical trials. These challenges are largely attributed to factors within the hostile TME. Our
518 ability to integrate multiple functional enhancements within a single construct that can still be
519 manufactured marks a substantial step forward in the field. Moreover, our findings extend
520 beyond treating GBM, as they can serve as standalone armoured modules for various CAR-T
521 constructs targeting different solid tumours. Demonstrating the feasibility of manufacturing

522 such a complex construct opens the door to incorporating diverse combinational elements
523 within a single CAR-T construct, allowing for tailored treatment strategies based on specific
524 cancer TMEs and antigens. Indeed, our data offers hope for more effective and safer treatments
525 for patients with GBM and other difficult-to-treat cancers.

526 **Limitations of the study**

527 Our research underscores the value of leveraging computational and in silico data in the design
528 of enhanced VHH CAR constructs. Although we demonstrate that this approach could
529 potentially reduce immunogenicity and enhance binding specificity, it is important to note that
530 our conclusions are derived from *in vitro* studies. Furthermore, while our multi-modular
531 strategy shows promise, it may also present limitations that require further investigation. We
532 have successfully demonstrated the safety and tolerability of our multi-armoured CAR-T
533 design in both *in vitro* cell culture systems and mouse models. However, it is crucial to
534 recognize that syngeneic mice and especially immunocompromised mouse models might differ
535 substantially from the actual human response and tolerability to cytokines such as IL-12. This
536 discrepancy highlights the need for caution when extrapolating our findings to human
537 applications. Finally, we demonstrated the feasibility of manufacturing our product, but it is
538 important to note that this process was conducted using specific conditions and may require
539 further optimization for large-scale production or clinical applications.

540 **RESOURCE AVAILABILITY**

541 **Lead contact:** Requests for further information and reagents should be directed to and will be
542 fulfilled by the Lead Contacts, Maurizio Mangolini (Maurizio.mangolini@chimeris.uk) and
543 Shimobi Onuoha (Shimobi.Onuoha@chimeris.uk)

Materials availability: All unique reagents generated in this study are listed in the manuscript and available from the lead contacts upon reasonable requests and a completed Materials Transfer Agreement.

Data and code availability: Transcriptomic data and accession codes will be made available upon manuscript's acceptance.

Acknowledgements:

We acknowledge the contribution of many people who contributed to this work either through useful discussions or the provision of reagents, including Agnieszka Andres and Dr Jun Li.

Author contributions:

Conception and experimental design: MM, SO, SS, SC, BM

Computational data generation: PS, SO, AR, MG

Experimental data generation: MM, ES, DP, SS, RK, YY, LS, HW

Analysis and interpretation of data: MM, SO, SS, SC, BM

Writing: MM, SO, SS, SC, PS

Competing interests:

Maurizio Mangolini, Saket Srivastava, Emily Souster, Yajing Yang, Rajesh Karattil, Liam Schultz, Biao Ma, Diana Pombal, Shaun Cordoba and Shimobi Onuoha are current (or former) employees of Chimeris Ltd and receive (or received) salary and shares for their work.

Maurizio Mangolini, Saket Srivastava, Emily Souster, Yajing Yang, Rajesh Karattil, Liam Schultz, Biao Ma, Shimobi Onuoha are inventors on patents filed on technologies presented in the manuscript.

The contribution to this study of Pietro Sormanni, Aubin Ramon and Matthew Greenig was conducted in a consultancy capacity and was remunerated by Chimeris UK.

567 **METHOD DETAILS**

568 **Primary cells and cell culture**

569 Peripheral Blood Mononuclear Cells (PBMCs) were isolated from Leukocyte Reduction
570 System (LRS) cones from consented platelet apheresis donors (NHSBT, Cambridge, UK) by
571 density centrifugation via Ficoll-Paque PLUS (GE-Healthcare; GE17-1440-03) according to
572 manufacturer protocol. Isolated PBMCs were cultured in complete RPMI (GIBCO,
573 ThermoFisher Scientific, Winsford, UK) supplemented with 10% Fetal Calf Serum (FBS)
574 (Labtech, Heathfield, UK), 2mM GlutaMAX (Gibco; 35050061), IL-7 and IL-15 at ng/mL
575 (Miltenyi Biotec, Germany).

576 Natural Killer (NK) cells were generated from isolated PBMCs using the CellXVivo Human
577 NK Cell Expansion Kit (Bio-techne, R&D System, Minneapolis, US) according to the
578 manufacturer's instructions.

579 Mouse splenocytes were isolated from spleens of 6- to 8-week-old C57BL/6 mice (Charles
580 River Laboratories).

581 HEK-293^{GP} and HEK-293^{RD114} (Biovec Pharma, Quebec City, Canada), Phoenix-ECO (ATCC;
582 ATCC®CRL-3214™) SNB19 (DMSZ, ACC 325 Leibniz Institute, Germany) lines were
583 cultured in Dulbecco's Modified Eagle Medium (DMEM) (GIBCO, ThermoFisher Scientific,
584 Winsford, UK) supplemented with 10% Fetal Calf Serum (FBS) (Labtech, Heathfield, UK) and
585 2mM GlutaMAX (Gibco; 35050061). HEK-Blue™ TGF-β and HEK-Blue™ IL-12 Cells
586 (InvivoGen, Toulouse, France) lines were cultured in complete DMEM supplemented with a
587 selection of antibiotics according to the manufacturer's instructions. SupT1 (ATCC;
588 ATCC®CRL-1942™) and Jurkat (Clone E6, ATCC; ATCC®TIB-152™) cells were cultured in
589 complete RPMI 1640 (GIBCO, ThermoFisher Scientific, Winsford, UK) supplemented with
590 10% FBS and 2mM GlutaMAX (Gibco; 35050061).

591 **Retroviral production and Transduction**

592 For amphotropic viral production, HEK-293GP cells were transiently transfected with a VSV-
593 G envelope expression plasmid and a retroviral cDNA construct (ratio 1:4). The transfection
594 was carried out with GeneJuice (Millipore; 70967-4) according to the manufacturer's
595 guidelines (ratio DNA:GeneJuice 1:2.5). After 72 h, the cell supernatant was filtered through a
596 0.45µM filter and the viral supernatant was added to HEK-293^{RD114} cells. Transduction was
597 performed by spinoculation (1500 × *g*, 1 h at 32 °C) with the addition of 10µg/ml Polybrene
598 (INSIGHT Biotechnology). Viral supernatant from HEK-293^{RD114} cells was then collected at
599 different time points when cell confluency reached ~100%, snap frozen and stored at -80 °C
600 for subsequent titration and use. Isolated PBMCs were activated using 10ng/ml IL-7 and IL-15
601 and 1:100 T Cell TransAct™ (Miltenyi Biotec). 48 hours post activation, 1x10^6 PBMCs were
602 plated on Retronectin (Takara Clonetech; T100B) on 6 well plates (Corning; 351146) with viral
603 supernatant and spun for 1500×*g*, 1 h at 32 °C.
604 For ecotropic viral production, Phoenix-ECO cells were transiently transfected with the pCL-
605 ECO packaging vector and a retroviral cDNA construct. After 72 h, the cell supernatant was
606 filtered through a 0.45µM filter and frozen. Isolated murine splenocytes were activated using
607 50ng/ml of aCD3 (Miltenyi Biotec; 130-093-387)/ aCD28 (Miltenyi Biotec; 130-093-375) and
608 50U/ml of mIL-2 (Miltenyi Biotec; 130-120-330). 24 hours post activation, cells were plated
609 on Retronectin (Takara Clonetech; T100B) on 6 well plates (Corning; 351146) with viral
610 supernatant and spun for 1500×*g*, 1h at 32 °C

611 **Flow Cytometry**

612 Flow cytometry was performed using a MACSQuant 10 flow cytometer (Miltenyi Biotec,
613 Germany). All labelling was conducted at room temperature (RT) for 15 minutes in subdued
614 light with antibodies diluted in PBS+2% FBS. The antibody used are: aCD3-PECy7
615 (BioLegend; 300420), aCD2-PE (BioLegend; 300208), aHA-APC (BioLegend; 901524),
616 aCD56-FITC (BioLegend; 318304), aCD8-FITC (BioLegend; 344704), aProtein L (Cell

617 Signalling, 29480L), pSTAT4-AF647 (BD Biosciences, Oxford, UK 558137) apSMAD2/3-
618 APC (BD Biosciences, Oxford, UK 562586), aHER2-FITC (R&D System, Minneapolis, US
619 FAB9589G).
620 IL13Rα2 CAR was detected using MonoRab™ Rabbit Anti-Camelid VHH Cocktail iFluor 647
621 (GenScript, Oxford,UK A02019-200).
622 Intracellular staining was performed using BD Phosflow™ Fix Buffer I and BD Phosflow™
623 Perm Buffer III (BD Biosciences, Oxford, UK) according to the manufacturer's protocol.

624 **Cytotoxicity assay**

625 Transduced cells were co-cultured with target cells at various effector:target (E:T) ratios, with
626 target cells remaining constant at $5x10^4$. Target cells are counted via flow cytometry using
627 CountBright Absolute Counting beads (Life Technologies; C36950) and cytotoxicity was
628 calculated as a percentage by normalising to the number of target cells recovered from co-
629 cultures with non-transduced (NT) T cells.

630 **Plate bound and re-stimulation assay**

631 Normalised T cells were cultured in 24-well plates previously coated overnight with 1ug/ml
632 IL13Rα2 protein and 1ug/ml TGF-β. 96h later cells were then co-cultured with SUPT1 target
633 cells and cytotoxicity was measured after 96h.
634 CAR T cells were seeded onto SNB19 cells and maintained for 7 days. Cells were harvested
635 and counted (Countess 3 Cell Counters, ThermoFisher Scientific, Winsford, UK). Cells were
636 then transferred to freshly plated SNB19 cells for repeat stimulation. 7 days later, T cells were
637 harvested, counted and finally co-cultured with SUPT1 target cells for cytotoxicity analysis at
638 the indicated E:T ratio.

639 **Cell-Free Protein Expression**

640 Proteins were produced using a cell-free expression system, specifically the PURExpress® 2.0
641 system (GeneFrontier Corporation), according to the manufacturer's protocol. Synthesized
642 constructs were derived from gBlocks® gene fragments (Integrated DNA Technologies),
643 designed to include a T7 promoter for transcription and a polyadenylation (poly A) tail for
644 stability. Each construct encoded a His-tag for subsequent purification. After transcription and
645 translation, the reaction mixtures were subjected to Ni-NTA affinity chromatography for
646 protein purification. The eluted proteins were concentrated and buffer exchanged using Amicon
647 Ultra centrifugal filters (MilliporeSigma) before downstream analyses. Protein purity and yield
648 were assessed via SDS-PAGE and Bradford assay.

649 **Mammalian Expression**

650 A separate set of proteins was produced in a mammalian expression system using the
651 pcDNA3.1(+) vector (Thermo Fisher Scientific). Constructs were designed to encode target
652 proteins fused with an Fc tag for improved stability and purification. Transient transfections
653 were performed in CHO-S cells (Thermo Fisher Scientific) cultured in CD CHO medium
654 supplemented with 8 mM L-glutamine and 1% HT supplement (Gibco). Transfections were
655 carried out using polyethylenimine (PEI) at a DNA:PEI ratio of 1:3. Following transfection,
656 cells were incubated for 5–7 days in a shaking incubator at 37°C with 5% CO_2 and 80%
657 humidity.

658 The proteins were harvested from the culture supernatant and purified using Protein A affinity
659 chromatography (GE Healthcare) under gravity flow. Eluted proteins were neutralized
660 immediately with 1 M Tris-HCl (pH 8.0) and subjected to buffer exchange into PBS using
661 Amicon Ultra centrifugal filters. The purity of the purified proteins was assessed using SDS-
662 PAGE, and concentrations were determined using a NanoDrop spectrophotometer (Thermo
663 Fisher Scientific). Proteins were stored at −80°C until further use.

664 **Binder Discovery and NGS sequence analysis**

665 NGS data were obtained from the MiSeq sequencing platform as two fastq files, one for
666 forward and one for reverse reads. These files were processed with an in-house python script
667 that merges forward and reverse reads assuming an overlapping region (which is always present
668 for short proteins like VHHs) to obtain the full sequence of the VHHs. The script further counts
669 the number of times each unique sequence is observed in the raw files (i.e., the number of reads
670 per unique sequence). Sequences were in silico translated to amino acids, and their count score
671 and corresponding frequency were used to sort the observed sequences from most to least
672 frequent, under the assumption that those sequences most abundant in the post-panning library
673 should be those binding most tightly to the target. All VHH sequences observed at least 3 times
674 (to reduce random sequencing errors) were aligned using the AHo numbering scheme as
675 described in [19]. The aligned CDR1, 2, and 3, were then combined and these joint CDR
676 sequences were used to determine homology groups. Specifically, each of the top 100
677 sequences by frequency in the library was considered as query, and its homology group
678 contained all sequences with a joint-CDR chemical distance smaller than 94, as calculated from
679 the distance matrix in Supplementary Figure 1a, which corresponds to around 25% CDR
680 sequence identity (this percent varies because e.g., a mutation R to K will have a much smaller
681 chemical distance than one from R to G). The assumption is that all sequences in a homology
682 group should engage the same epitope, given their highly similar CDRs. Overlapping
683 homology groups were merged. Figure 1c reports the percent frequency of the top-ranking
684 sequence used as query on the x-axis, and the sum of the percent frequencies of all sequences
685 in the homology group on the y-axis. Value labels are the ranking of the top sequence in the
686 library, with 0 corresponding to the highest frequency sequence.

687 **In vivo studies**

688 Animal studies were performed under a UK Home Office–approved project license.

689 Crown Bioscience UK Ltd carried out C57BL/6 animal studies. In brief, $1x10^5$ B16.F10 cells,
690 modified to express GD2, were subcutaneously injected into 6–10-week-old C57BL/6 female
691 mice. Eight days post engraftment $2.5x10^6$ CAR T-cells were injected intravenously and mice
692 were monitored for body weight and tumor volume using a caliper. Mice were randomized one
693 day pre-tumor injection and one day prior to treatment.
694 $5x10^4$ U87 cells, modified to express hIL13Rα2, were inoculated intracranially into NSG mice.
695 On day 7 Tumour engraftment was measured by bioluminescent imaging utilizing the IVIS
696 spectrum system (PerkinElmer, Waltham, MA) after intra-luciferin peritoneal injection and
697 mice were randomized for CAR treatment. The following day, $6.25x10^4$ CAR T-cells were
698 injected intracranially. For the subcutaneous model, mice were subcutaneously injected with 1
699 $\times 10^7$ U87-IL13Rα2 cells. CAR-T cells were administered intravenously when tumors reached
700 ~200 mm^3.
701 **Statistical analysis**
702 Data analyses were performed using GraphPad Prism 10 (GraphPad Software, La Jolla, USA)
703 with paired analyses as indicated. For experiments where more than two groups are compared,
704 statistical analyses were performed using one-way ANOVA followed by two-tail Student t-
705 tests. Statistical annotations were denoted with asterisks as follows: ****$P < 0.0001$,
706 ***$P < 0.001$, **$P < 0.01$, *$P < 0.05$, and not significant (ns) $P > 0.05$.

REFERENCES

1. Wu, W., Klockow, J.L., Zhang, M., Lafortune, F., Chang, E., Jin, L., Wu, Y., and Daldrup-Link, H.E. (2021). Glioblastoma multiforme (GBM): An overview of current therapies and mechanisms of resistance. Pharmacol. Res. *171*, 105780. https://doi.org/10.1016/j.phrs.2021.105780.

2. Rodgers, L.T., Villano, J.L., Hartz, A.M.S., and Bauer, B. (2024). Glioblastoma Standard of Care: Effects on Tumor Evolution and Reverse Translation in Preclinical Models. Cancers *16*, 2638. https://doi.org/10.3390/cancers16152638.

3. Land, C.A., Musich, P.R., Haydar, D., Krenciute, G., and Xie, Q. (2020). Chimeric antigen receptor T-cell therapy in glioblastoma: charging the T cells to fight. J. Transl. Med. *18*, 428. https://doi.org/10.1186/s12967-020-02598-0.

4. Wykosky, J., Gibo, D.M., Stanton, C., and Debinski, W. (2008). Interleukin-13 receptor alpha 2, EphA2, and Fos-related antigen 1 as molecular denominators of high-grade astrocytomas and specific targets for combinatorial therapy. Clin. Cancer Res. Off. J. Am. Assoc. Cancer Res. *14*, 199–208. https://doi.org/10.1158/1078-0432.CCR-07-1990.

5. Zeng, J., Zhang, J., Yang, Y.-Z., Wang, F., Jiang, H., Chen, H.-D., Wu, H.-Y., Sai, K., and Hu, W.-M. (2020). IL13RA2 is overexpressed in malignant gliomas and related to clinical outcome of patients. Am. J. Transl. Res. *12*, 4702–4714.

6. Saikali, S., Avril, T., Collet, B., Hamlat, A., Bansard, J.-Y., Drenou, B., Guegan, Y., and Quillien, V. (2007). Expression of nine tumour antigens in a series of human glioblastoma multiforme: interest of EGFRvIII, IL-13Ralpha2, gp100 and TRP-2 for immunotherapy. J. Neurooncol. *81*, 139–148. https://doi.org/10.1007/s11060-006-9220-3.

7. Brown, C.E., Warden, C.D., Starr, R., Deng, X., Badie, B., Yuan, Y.-C., Forman, S.J., and Barish, M.E. (2013). Glioma IL13Rα2 Is Associated with Mesenchymal Signature Gene Expression and Poor Patient Prognosis. PLoS ONE *8*, e77769. https://doi.org/10.1371/journal.pone.0077769.

8. Brown, C.E., Badie, B., Barish, M.E., Weng, L., Ostberg, J.R., Chang, W.-C., Naranjo, A., Starr, R., Wagner, J., Wright, C., et al. (2015). Bioactivity and Safety of IL13Rα2-Redirected Chimeric Antigen Receptor CD8+ T Cells in Patients with Recurrent Glioblastoma. Clin. Cancer Res. *21*, 4062–4072. https://doi.org/10.1158/1078-0432.CCR-15-0428.

9. Brown, C.E., Alizadeh, D., Starr, R., Weng, L., Wagner, J.R., Naranjo, A., Ostberg, J.R., Blanchard, M.S., Kilpatrick, J., Simpson, J., et al. (2016). Regression of Glioblastoma after Chimeric Antigen Receptor T-Cell Therapy. N. Engl. J. Med. *375*, 2561–2569. https://doi.org/10.1056/NEJMoa1610497.

10. Bagley, S.J., Logun, M., Fraietta, J.A., Wang, X., Desai, A.S., Bagley, L.J., Nabavizadeh, A., Jarocha, D., Martins, R., Maloney, E., et al. (2024). Intrathecal

bivalent CAR T cells targeting EGFR and IL13Rα2 in recurrent glioblastoma: phase 1 trial interim results. Nat. Med. *30*, 1320–1329. https://doi.org/10.1038/s41591-024-02893-z.

11. Brown, C.E., Hibbard, J.C., Alizadeh, D., Blanchard, M.S., Natri, H.M., Wang, D., Ostberg, J.R., Aguilar, B., Wagner, J.R., Paul, J.A., et al. (2024). Locoregional delivery of IL-13Rα2-targeting CAR-T cells in recurrent high-grade glioma: a phase 1 trial. Nat. Med. *30*, 1001–1012. https://doi.org/10.1038/s41591-024-02875-1.

12. Yang, L., Pang, Y., and Moses, H.L. (2010). TGF-beta and immune cells: an important regulatory axis in the tumor microenvironment and progression. Trends Immunol. *31*, 220–227. https://doi.org/10.1016/j.it.2010.04.002.

13. Thomas, D.A., and Massagué, J. (2005). TGF-beta directly targets cytotoxic T cell functions during tumor evasion of immune surveillance. Cancer Cell *8*, 369–380. https://doi.org/10.1016/j.ccr.2005.10.012.

14. Kloss, C.C., Lee, J., Zhang, A., Chen, F., Melenhorst, J.J., Lacey, S.F., Maus, M.V., Fraietta, J.A., Zhao, Y., and June, C.H. (2018). Dominant-Negative TGF-β Receptor Enhances PSMA-Targeted Human CAR T Cell Proliferation And Augments Prostate Cancer Eradication. Mol. Ther. J. Am. Soc. Gene Ther. *26*, 1855–1866. https://doi.org/10.1016/j.ymthe.2018.05.003.

15. Car, B.D., Eng, V.M., Lipman, J.M., and Anderson, T.D. (1999). The Toxicology of Interleukin-12: A Review. Toxicol. Pathol. *27*, 58–63. https://doi.org/10.1177/019262339902700112.

16. Jenks, S. (1996). After Initial Setback, IL-12 Regaining Popularity. JNCI J. Natl. Cancer Inst. *88*, 576–577. https://doi.org/10.1093/jnci/88.9.576.

17. Jia, Z., Ragoonanan, D., Mahadeo, K.M., Gill, J., Gorlick, R., Shpal, E., and Li, S. (2022). IL12 immune therapy clinical trial review: Novel strategies for avoiding CRS-associated cytokines. Front. Immunol. *13*, 952231. https://doi.org/10.3389/fimmu.2022.952231.

18. Asaadi, Y., Jouneghani, F.F., Janani, S., and Rahbarizadeh, F. (2021). A comprehensive comparison between camelid nanobodies and single chain variable fragments. Biomark. Res. *9*, 87. https://doi.org/10.1186/s40364-021-00332-6.

19. Ramon, A., Ali, M., Atkinson, M., Saturnino, A., Didi, K., Visentin, C., Ricagno, S., Xu, X., Greenig, M., and Sormanni, P. (2024). Assessing antibody and nanobody nativeness for hit selection and humanization with AbNatiV. Nat. Mach. Intell. *6*, 74–91. https://doi.org/10.1038/s42256-023-00778-3.

20. Marofi, F., Motavalli, R., Safonov, V.A., Thangavelu, L., Yumashev, A.V., Alexander, M., Shomali, N., Chartrand, M.S., Pathak, Y., Jarahian, M., et al. (2021). CAR T cells in solid tumors: challenges and opportunities. Stem Cell Res. Ther. *12*, 81. https://doi.org/10.1186/s13287-020-02128-1.

21. Yang, L., Pang, Y., and Moses, H.L. (2010). TGF-beta and immune cells: an important regulatory axis in the tumor microenvironment and progression. Trends Immunol. *31*, 220–227. https://doi.org/10.1016/j.it.2010.04.002.

22. Han, J., Alvarez-Breckenridge, C.A., Wang, Q.-E., and Yu, J. (2015). TGF-β signaling and its targeting for glioma treatment. Am. J. Cancer Res. *5*, 945–955.

23. Golán-Cancela, I., and Caja, L. (2024). The TGF-β Family in Glioblastoma. Int. J. Mol. Sci. *25*, 1067. https://doi.org/10.3390/ijms25021067.

24. Tugues, S., Burkhard, S.H., Ohs, I., Vrohlings, M., Nussbaum, K., Vom Berg, J., Kulig, P., and Becher, B. (2015). New insights into IL-12-mediated tumor suppression. Cell Death Differ. *22*, 237–246. https://doi.org/10.1038/cdd.2014.134.

25. Lieschke, G.J., Rao, P.K., Gately, M.K., and Mulligan, R.C. (1997). Bioactive murine and human interleukin-12 fusion proteins which retain antitumor activity in vivo. Nat. Biotechnol. *15*, 35–40. https://doi.org/10.1038/nbt0197-35.

26. Chen, X., Zaro, J.L., and Shen, W.-C. (2013). Fusion protein linkers: property, design and functionality. Adv. Drug Deliv. Rev. *65*, 1357–1369. https://doi.org/10.1016/j.addr.2012.09.039.

27. Glassman, C.R., Mathiharan, Y.K., Jude, K.M., Su, L., Panova, O., Lupardus, P.J., Spangler, J.B., Ely, L.K., Thomas, C., Skiniotis, G., et al. (2021). Structural basis for IL-12 and IL-23 receptor sharing reveals a gateway for shaping actions on T versus NK cells. Cell *184*, 983-999.e24. https://doi.org/10.1016/j.cell.2021.01.018.

28. Bloch, Y., Felix, J., Merceron, R., Provost, M., Symakani, R.A., De Backer, R., Lambert, E., Mehdipour, A.R., and Savvides, S.N. (2024). Structures of complete extracellular receptor assemblies mediated by IL-12 and IL-23. Nat. Struct. Mol. Biol. *31*, 591–597. https://doi.org/10.1038/s41594-023-01190-6.

29. Lee, E.H.J., Murad, J.P., Christian, L., Gibson, J., Yamaguchi, Y., Cullen, C., Gumber, D., Park, A.K., Young, C., Monroy, I., et al. (2023). Antigen-dependent IL-12 signaling in CAR T cells promotes regional to systemic disease targeting. Nat. Commun. *14*, 4737. https://doi.org/10.1038/s41467-023-40115-1.

30. Sahillioglu, A.C., and Schumacher, T.N. (2022). Safety switches for adoptive cell therapy. Curr. Opin. Immunol. *74*, 190–198. https://doi.org/10.1016/j.coi.2021.07.002.

31. García-Alonso, S., Ocaña, A., and Pandiella, A. (2020). Trastuzumab Emtansine: Mechanisms of Action and Resistance, Clinical Progress, and Beyond. Trends Cancer *6*, 130–146. https://doi.org/10.1016/j.trecan.2019.12.010.

32. Voisinne, G., Gonzalez de Peredo, A., and Roncagalli, R. (2018). CD5, an Undercover Regulator of TCR Signaling. Front. Immunol. *9*, 2900. https://doi.org/10.3389/fimmu.2018.02900.

33. Bulcha, J.T., Wang, Y., Ma, H., Tai, P.W.L., and Gao, G. (2021). Viral vector platforms within the gene therapy landscape. Signal Transduct. Target. Ther. *6*, 53. https://doi.org/10.1038/s41392-021-00487-6.

34. Sandrin, V., Boson, B., Salmon, P., Gay, W., Nègre, D., Le Grand, R., Trono, D., and Cosset, F.-L. (2002). Lentiviral vectors pseudotyped with a modified RD114 envelope glycoprotein show increased stability in sera and augmented transduction of primary lymphocytes and CD34+ cells derived from human and nonhuman primates. Blood *100*, 823–832. https://doi.org/10.1182/blood-2001-11-0042.

35. Ghani, K., Cottin, S., De Campos-Lima, P.O., Caron, M., and Caruso, M. (2009). Characterization of an alternative packaging system derived from the cat RD114 retrovirus for gene delivery. J. Gene Med. *11*, 664–669. https://doi.org/10.1002/jgm.1351.

36. Gumber, D., and Wang, L.D. (2022). Improving CAR-T immunotherapy: Overcoming the challenges of T cell exhaustion. eBioMedicine *77*, 103941. https://doi.org/10.1016/j.ebiom.2022.103941.

37. Candolfi, M., Curtin, J.F., Nichols, W.S., Muhammad, A.G., King, G.D., Pluhar, G.E., McNiel, E.A., Ohlfest, J.R., Freese, A.B., Moore, P.F., et al. (2007). Intracranial glioblastoma models in preclinical neuro-oncology: neuropathological characterization and tumor progression. J. Neurooncol. *85*, 133–148. https://doi.org/10.1007/s11060-007-9400-9.

38. Ludwig, J., and Hirschel, M. (2020). Methods and Process Optimization for Large-Scale CAR T Expansion Using the G-Rex Cell Culture Platform. In Chimeric Antigen Receptor T Cells Methods in Molecular Biology., K. Swiech, K. C. R. Malmegrim, and V. Picanço-Castro, eds. (Springer US), pp. 165–177. https://doi.org/10.1007/978-1-0716-0146-4_12.

39. Center for Biologics Evaluation and Research OTAT Town Hall: Gene Therapy Chemistry, Manufacturing, and Controls.

40. Sallusto, F., Geginat, J., and Lanzavecchia, A. (2004). Central Memory and Effector Memory T Cell Subsets: Function, Generation, and Maintenance. Annu. Rev. Immunol. *22*, 745–763. https://doi.org/10.1146/annurev.immunol.22.012703.104702.

41. Kahlon, K.S., Brown, C., Cooper, L.J.N., Raubitschek, A., Forman, S.J., and Jensen, M.C. (2004). Specific Recognition and Killing of Glioblastoma Multiforme by Interleukin 13-Zetakine Redirected Cytolytic T Cells. Cancer Res. *64*, 9160–9166. https://doi.org/10.1158/0008-5472.CAN-04-0454.

42. Krebs, S., Chow, K.K.H., Yi, Z., Rodriguez-Cruz, T., Hegde, M., Gerken, C., Ahmed, N., and Gottschalk, S. (2014). T cells redirected to interleukin-13Rα2 with interleukin-13 mutein–chimeric antigen receptors have anti-glioma activity but also recognize interleukin-13Rα1. Cytotherapy *16*, 1121–1131. https://doi.org/10.1016/j.jcyt.2014.02.012.

43. Brown, C.E., Aguilar, B., Starr, R., Yang, X., Chang, W.-C., Weng, L., Chang, B., Sarkissian, A., Brito, A., Sanchez, J.F., et al. (2018). Optimization of IL13Rα2-Targeted Chimeric Antigen Receptor T Cells for Improved Anti-tumor Efficacy against Glioblastoma. Mol. Ther. *26*, 31–44. https://doi.org/10.1016/j.ymthe.2017.10.002.

44. Krenciute, G., Krebs, S., Torres, D., Wu, M.-F., Liu, H., Dotti, G., Li, X.-N., Lesniak, M.S., Balyasnikova, I.V., and Gottschalk, S. (2016). Characterization and Functional Analysis of scFv-based Chimeric Antigen Receptors to Redirect T Cells to IL13Rα2-positive Glioma. Mol. Ther. *24*, 354–363. https://doi.org/10.1038/mt.2015.199.

45. Choi, B.D., Gerstner, E.R., Frigault, M.J., Leick, M.B., Mount, C.W., Balaj, L., Nikiforow, S., Carter, B.S., Curry, W.T., Gallagher, K., et al. (2024). Intraventricular CARv3-TEAM-E T Cells in Recurrent Glioblastoma. N. Engl. J. Med. *390*, 1290–1298. https://doi.org/10.1056/NEJMoa2314390.

46. Turley, S.J., Cremasco, V., and Astarita, J.L. (2015). Immunological hallmarks of stromal cells in the tumour microenvironment. Nat. Rev. Immunol. *15*, 669–682. https://doi.org/10.1038/nri3902.

47. Tang, N., Cheng, C., Zhang, X., Qiao, M., Li, N., Mu, W., Wei, X.-F., Han, W., and Wang, H. (2020). TGF-β inhibition via CRISPR promotes the long-term efficacy of CAR T cells against solid tumors. JCI Insight *5*, e133977. https://doi.org/10.1172/jci.insight.133977.

48. DeRenzo, C., and Gottschalk, S. (2019). Genetic Modification Strategies to Enhance CAR T Cell Persistence for Patients With Solid Tumors. Front. Immunol. *10*, 218. https://doi.org/10.3389/fimmu.2019.00218.

49. Shum, T., Omer, B., Tashiro, H., Kruse, R.L., Wagner, D.L., Parikh, K., Yi, Z., Sauer, T., Liu, D., Parihar, R., et al. (2017). Constitutive Signaling from an Engineered IL7 Receptor Promotes Durable Tumor Elimination by Tumor-Redirected T Cells. Cancer Discov. *7*, 1238–1247. https://doi.org/10.1158/2159-8290.CD-17-0538.

50. Lin, F.Y., Stuckert, A., Tat, C., White, M., Ruggieri, L., Zhang, H., Mehta, B., Lapteva, N., Mei, Z., Major, A., et al. (2024). Phase I Trial of GD2.CART Cells Augmented With Constitutive Interleukin-7 Receptor for Treatment of High-Grade Pediatric CNS Tumors. J. Clin. Oncol. *42*, 2769–2779. https://doi.org/10.1200/JCO.23.02019.

51. Seder, R.A., Gazzinelli, R., Sher, A., and Paul, W.E. (1993). Interleukin 12 acts directly on CD4+ T cells to enhance priming for interferon gamma production and diminishes interleukin 4 inhibition of such priming. Proc. Natl. Acad. Sci. *90*, 10188–10192. https://doi.org/10.1073/pnas.90.21.10188.

52. Gazzinelli, R.T., Wysocka, M., Hayashi, S., Denkers, E.Y., Hieny, S., Caspar, P., Trinchieri, G., and Sher, A. (1994). Parasite-induced IL-12 stimulates early IFN-gamma synthesis and resistance during acute infection with Toxoplasma gondii. J. Immunol. Baltim. Md 1950 *153*, 2533–2543.

53. Lasek, W., Zagożdżon, R., and Jakobisiak, M. (2014). Interleukin 12: still a promising candidate for tumor immunotherapy? Cancer Immunol. Immunother. CII *63*, 419–435. https://doi.org/10.1007/s00262-014-1523-1.

54. Zhang, L., Morgan, R.A., Beane, J.D., Zheng, Z., Dudley, M.E., Kassim, S.H., Nahvi, A.V., Ngo, L.T., Sherry, R.M., Phan, G.Q., et al. (2015). Tumor-Infiltrating Lymphocytes Genetically Engineered with an Inducible Gene Encoding Interleukin-12 for the Immunotherapy of Metastatic Melanoma. Clin. Cancer Res. *21*, 2278–2288. https://doi.org/10.1158/1078-0432.CCR-14-2085.

55. Zhang, L., Davies, J.S., Serna, C., Yu, Z., Restifo, N.P., Rosenberg, S.A., Morgan, R.A., and Hinrichs, C.S. (2020). Enhanced efficacy and limited systemic cytokine exposure with membrane-anchored interleukin-12 T-cell therapy in murine tumor models. J. Immunother. Cancer *8*, e000210. https://doi.org/10.1136/jitc-2019-000210.

56. Hu, J., Yang, Q., Zhang, W., Du, H., Chen, Y., Zhao, Q., Dao, L., Xia, X., Natalie Wall, F., Zhang, Z., et al. (2022). Cell membrane-anchored and tumor-targeted IL-12 (attIL12)-T cell therapy for eliminating large and heterogeneous solid tumors. J. Immunother. Cancer *10*, e003633. https://doi.org/10.1136/jitc-2021-003633.

57. Lee, E.H.J., Murad, J.P., Christian, L., Gibson, J., Yamaguchi, Y., Cullen, C., Gumber, D., Park, A.K., Young, C., Monroy, I., et al. (2023). Antigen-dependent IL-12 signaling in CAR T cells promotes regional to systemic disease targeting. Nat. Commun. *14*, 4737. https://doi.org/10.1038/s41467-023-40115-1.

58. Zhou, X., Dotti, G., Krance, R.A., Martinez, C.A., Naik, S., Kamble, R.T., Durett, A.G., Dakhova, O., Savoldo, B., Di Stasi, A., et al. (2015). Inducible caspase-9 suicide gene controls adverse effects from alloreplete T cells after haploidentical stem cell transplantation. Blood *125*, 4103–4113. https://doi.org/10.1182/blood-2015-02-628354.

59. Del Bufalo, F., De Angelis, B., Caruana, I., Del Baldo, G., De Ioris, M.A., Serra, A., Mastronuzzi, A., Cefalo, M.G., Pagliara, D., Amicucci, M., et al. (2023). GD2-CART01 for Relapsed or Refractory High-Risk Neuroblastoma. N. Engl. J. Med. *388*, 1284–1295. https://doi.org/10.1056/NEJMoa2210859.

60. Diaconu, I., Ballard, B., Zhang, M., Chen, Y., West, J., Dotti, G., and Savoldo, B. (2017). Inducible Caspase-9 Selectively Modulates the Toxicities of CD19-Specific Chimeric Antigen Receptor-Modified T Cells. Mol. Ther. J. Am. Soc. Gene Ther. *25*, 580–592. https://doi.org/10.1016/j.ymthe.2017.01.011.

935 **STAR★METHODS**

936 KEY RESOURCES TABLE

937

REAGENT OR RESOURCE	SOURCE	IDENTIFIER
Antibodies		
CD3-PECy7	BioLegend	300420
CD2-PE	BioLegend	300208
HA-APC	BioLegend	901524
CD56-FITC	BioLegend	318304
CD8-FITC	BioLegend	344704
Protein L	Cell Signalling	29480L
pSTAT4-AF647	BD Biosciences	558137
pSMAD2/3-APC	BD Biosciences	562586
HER2-FITC	R&D System	FAB9589G
MonoRab™ Rabbit Anti-Camelid VHH Cocktail iFluor 647	GenScript	A02019-200
Biological samples		
Human peripheral blood mononuclear cells (PBMCs)	Healthy donors	
Chemicals, peptides, and recombinant proteins		
Recombinant Human IL-12 R beta 1 Fc Chimera Protein	R&D System	839-B1-100
Recombinant Human IL-12 R beta 2 Fc Chimera Protein	R&D System	1959-B2B-050
Trastuzumab Emtansine	Selleck Biotechnology Limited	D4003-1mg
Recombinant Human TGF-beta 1 Protein	R&D System	240-B-002/CF
rhIL7	Miltenyi Biotec	130-095-367
rhIL15	Miltenyi Biotec	130-095-760
GeneJuice	Millipore	70967-4
Retronectin	Takara	T100B
T cell Transact	Miltenyi Biotec	130-111-160
scIL-12 variants	This paper	
Critical commercial assays		
CellTrace CFSE	ThermoFisher Scientific	C34557
Human IFN-γ ELISA Kit	Biolegend	430104
Human IL2 ELISA Kit	Biolegend	431804
Annexin V Apoptosis Detection Kit	Biolegend	640932
CellXVivo Human NK Cell Expansion Kit	Bio-techne R&D System	CDK015
BD Cytofix/Cytoperm™ Fixation/Permeabilization Kit	BD Biosciences	554714
Experimental models: Cell lines		
Phoenix-ECO	ATCC	CRL-3214
SupT1	ATCC	CRL-1942
Jurkat	ATCC	TIB-152
B16.F10	ATCC	CRL-6475
SNB19	DMSZ	ACC 325
HEK-Blue™ TGF-β	InvivoGen	hkb-tgfbv2

HEK-Blue™ IL-12	InvivoGen	hkb-il12
HEK-293GP	Biovec Pharma	
HEK-293RD114	Biovec Pharma	
Experimental models: Organisms/strains		
NOD.Cg-PrkdcSCID Il2rgtm1Wjl/SzJ (NSG) mice	The Jackson Laboratory	
C57BL/6NCrl	The Jackson Laboratory	
Recombinant DNA		
IL13Rα2 CAR	This paper	
scIL-12	This paper	
dsFvTBRII/CCR	This paper	
HER2	This paper	
Software and algorithms		
FlowJo 10.0	FlowJo, LLC	https://www.flowjo.com/
Prism 10	GraphPad	https://www.graphpad.com
BioRender	BioRender	https://www.biorender.com/

Figure 1 : *In vitro* screening identifies lead IL13Rα2 VHH for CAR-T cells

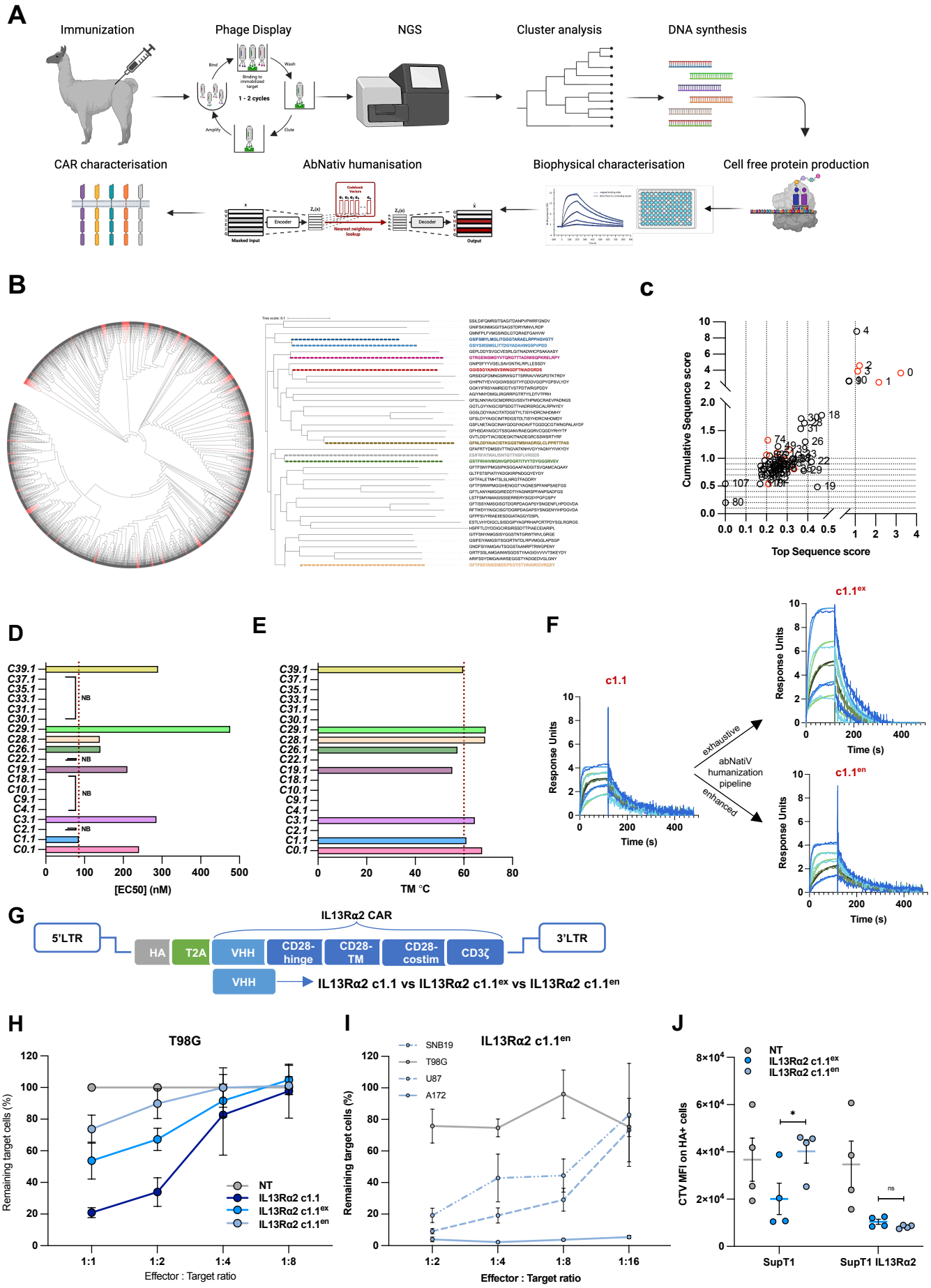

Figure 1: *In vitro* screening identifies lead IL13Rα2 VHH for CAR-T cells.

A. Graphical scheme of the experimental procedures to identify a new IL13Ra2 VHH for CAR-T cells created with BioRender.com. **B**. Phylogenetic tree generated using iTol, illustrating the complete library diversity. Clusters identified during analysis are highlighted in red. Clusters were determined by concatenating the three CDRs and analysing their diversity using a chemical space distance matrix. The sequences of the top clusters were further analysed in a unique tree to explore the distances between the combined CDRs of the highest-represented clones within the diverse clusters. **C**. Analysis of potential library bias during panning, represented as a plot of the top sequence score against the cumulative sequence score, highlighting the enrichment dynamics and selection preferences. Bar plots of the binding values (**D**) and the apparent melting temperatures (**e**) of the selected clones produced using cell-free based expression system. Values are representative measurements from three independent replicates. NB: non-binding. **F**. Binding sensorgrams of respective representative measurements showing the binding of c1.1, c.1.1^{en} and c1.1^{ex} to human IL13Rα2 by SPR. IL13Rα2 c1.1^{ex} and IL13Rα2 c1.1^{en} are based on the selected c1.1 clone and humanised using the exhaustive (^{ex}) or enhanced (^{en}) abNatiV pipeline. **G.** Schematic representation of CAR-T vectors targeting IL13Rα2. The vectors comprise an N-terminal HA-tag serving as a transduction marker, followed by the anti-IL13Rα2 VHH of interest. The VHH is linked to the transmembrane and intracellular regions of the CD28 signalling domain, which is then connected to the CD3ζ signalling domain. LTR, long terminal repeat.

H,I. Different glioma cell lines were co-cultured with different ratios of CAR-T cells for 72 hours. Viable target cells were quantified by flow cytometry using CD2 and CD3 expression as exclusion markers. The percentage of live target cells was calculated by normalizing to the NT group. **J**. Antigen-specific proliferation was determined by co-culturing CTV-labeled T cells with SupT1-IL13Rα2 or SupT1 cells for 96 hours. The T cells were either untransduced (NT) or expressing the IL13Rα2 c1.1^{en} or IL13Rα2 c1.1^{ex} CAR vector. *$P < 0.05$, **$P < 0.01$, ***$P < 0.001$, ****$P < 0.0001$ and not significant (ns) $P > 0.05$.

Figure 2: dsFvTBRII/CCR overcomes the inhibitory effects of TGF-β and induces CAR-T cell persistence.

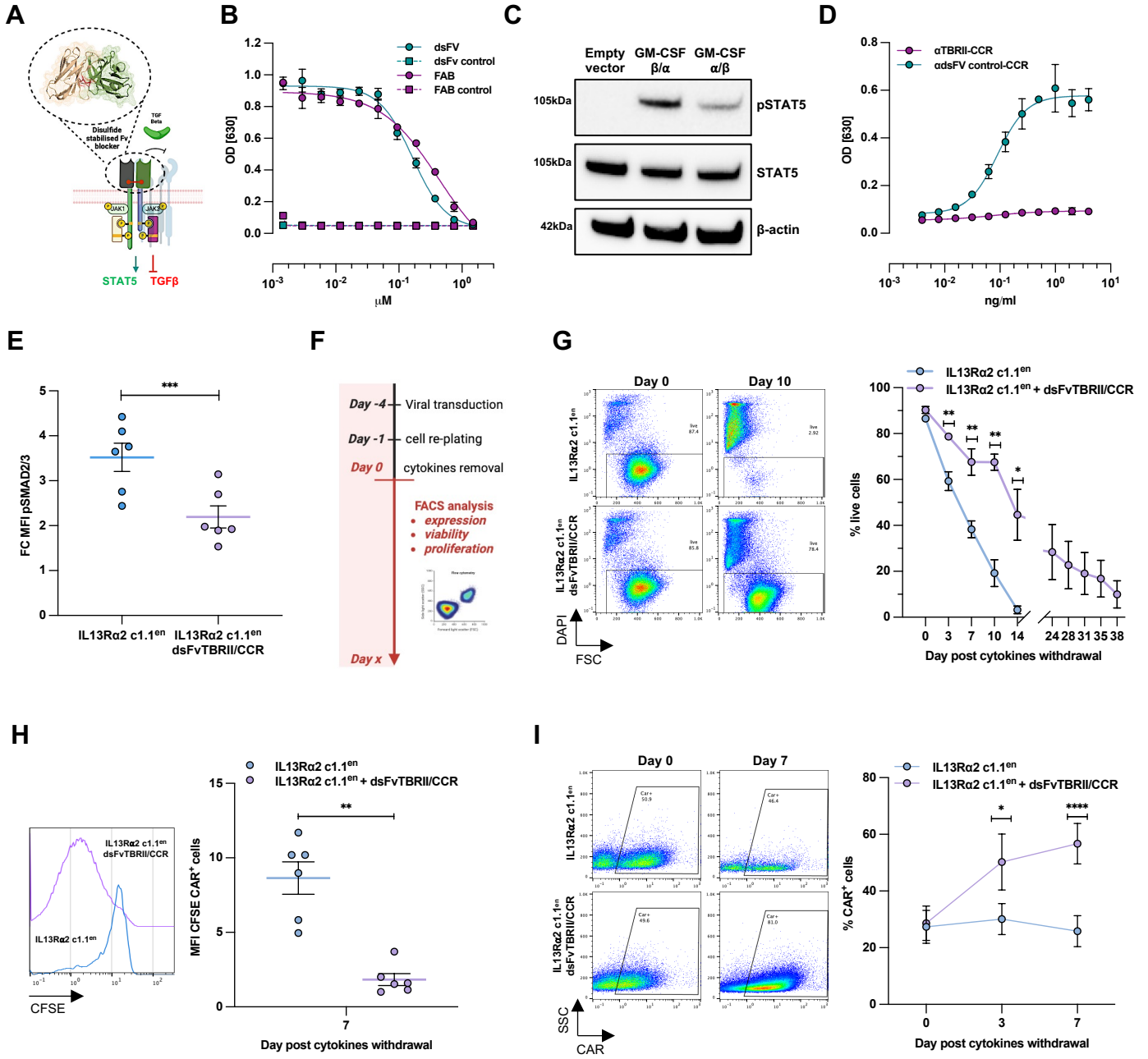

Figure 2: dsFvTBRII/CCR overcomes the inhibitory effects of TGF-β and induces CAR-T cell persistence.

A. Graphical scheme of the dsFvTBRII/CCR construct. **B.** Quantification of the SEAP secreted by HEK-Blue™ TGF-β cultured in the presence of TGF-β and the indicated level of the different TBRII blocking antibodies. **C.** Analysis of phospho-STAT5 and total STAT5 levels in Jurkat cells expressing the dsFvTBRII region fused with different orientations of the GM-CSF receptor chains: alpha-beta and beta-alpha. **D.** Quantification of the SEAP secreted by HEK-Blue™ TGF-β cultured in the presence of TGF-β and the indicated level of dsFvTBRII/CCR or a non-targeting/CCR control antibody. **E.** Quantification of intracellular phospho-SMAD2/3 levels by flow cytometry in T cells expressing IL13Ra2 c1.1^{en} CAR or IL13Ra2 c1.1^{en} CAR+dsFvTBRII/CCR exposed to 10ng/ml TGF-β for 30'. Cells were grown in serum-free media overnight before TGF-β stimulation. **F.** Schematic representation of the experimental setup. **G.** Percentage of live IL13Ra2 c1.1^{en} CAR or IL13Ra2 c1.1^{en} CAR+dsFvTBRII/CCR cells following cytokine withdrawal (n=6). Live cells were identified by DAPI exclusion by flow cytometry. **H.** Measurement of transduced T-cell proliferation by CFSE dilution 7 days post cytokine withdrawal (n=6). Cells were labelled with CFSE at day 0. **i.** Analysis of CAR-positive cell enrichment over time following cytokine withdrawal measured by flow cytometry (n=6). A representative flow cytometry plot from an individual T cell donor is presented for **G**,**H**,**I**. Cohorts are shown as mean ± SEM. Statistical analysis was done by paired t-tests. *$P < 0.05$, **$P < 0.01$, ***$P < 0.001$, ****$P < 0.0001$ and not significant (ns) $P > 0.05$. **A**,**F** were created with BioRender.com

Figure 3: scIL12^{inv} demonstrates enhanced safety while preserving its potent anti-cancer effects

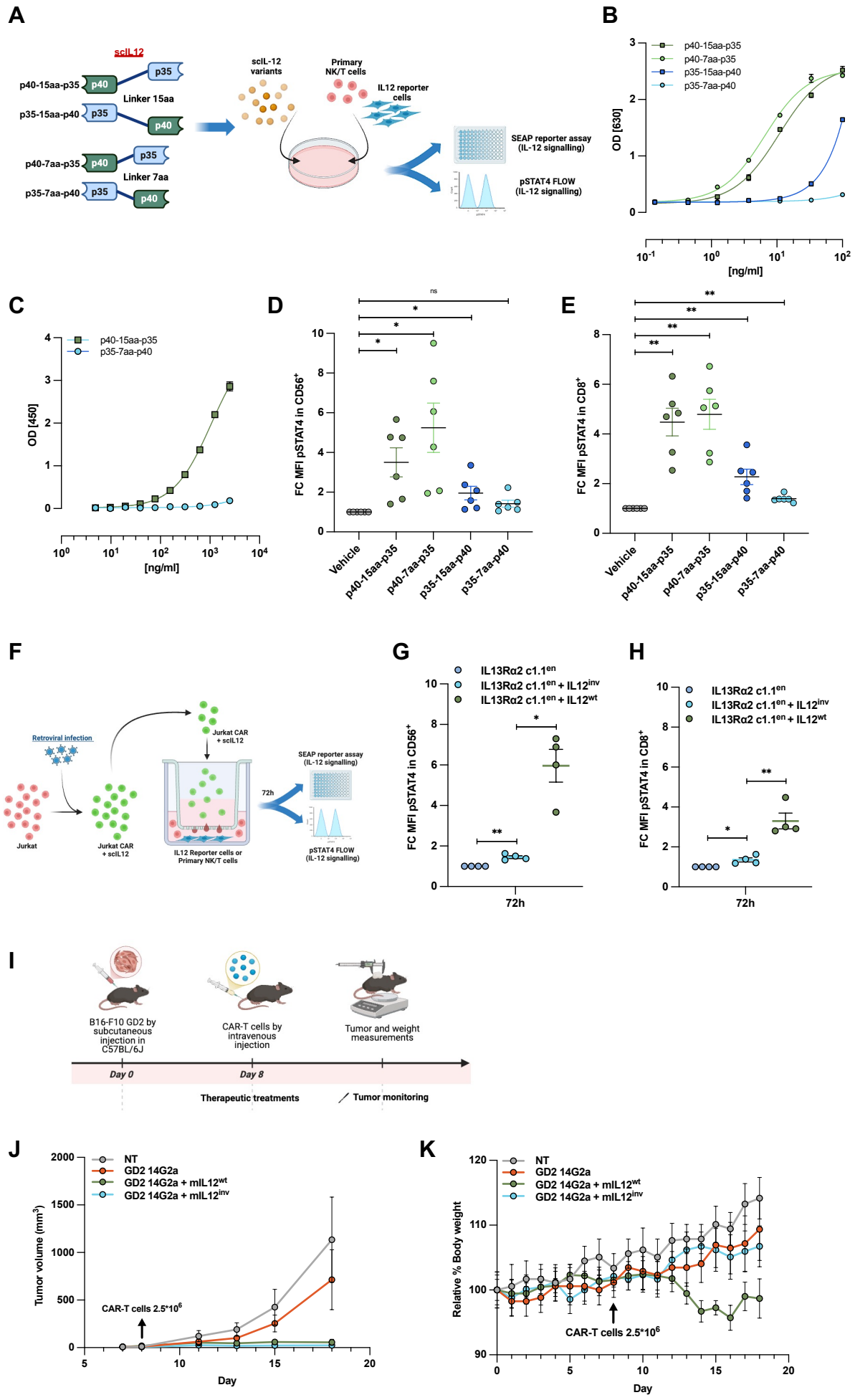

Figure 3: IL12^{inv} demonstrates enhanced safety while preserving its potent anti-cancer effects

A. Schematic representation of the protein used and the experimental layout. **b.** Quantification of the SEAP secreted by HEK-Blue™ IL12 cultured in the presence of scIL12 purified recombinant proteins at the indicated concentration for 72h. **C.** Affinity of the designed p40-15aa-p35 and p35-7aa-p40 scIL12s to the immobilized IL12β1 evaluated by ELISA assay. scIL12s were detected using an α-HIS-HRP conjugated antibody. **D,E.** CD56$^+$ and CD8$^+$ cell assay demonstrating signalling capacity of scIL-12 variants using purified recombinant protein at 100ng/ml for 30 minutes. Cells were harvested, fixed and permeabilised to detect pSTAT4 status by flow cytometry. T cells were previously activated with αCD3/CD28 in the presence of IL-2. **F.** Schematic representation of the experimental layout. **G,H.** pSTAT4 level in CD56$^+$ and CD8$^+$ cells following co-culture with Jurkat cells expressing IL13Rα2 c1.1^{en}, IL13Rα2 c1.1^{en}+IL12^{inv} or IL13Rα2 c1.1^{en}+IL12^{inv} CAR for 72h. Cells were co-cultured using a 0.4µm cell-permeable culture support. **i.** Schematic representation of the *in vivo* experimental layout created with BioRender.com. Tumor volume (**J**) and body weight (**K**) measurements of mice subcutaneously injected with 1x10^5 GD2-expressing B16.F10 cells, which were allowed to engraft for 8 days before a 2.5x10^6 dose of non-transduced T or CAR-T cells was intravenously injected via the tail vein. Cohorts are shown as mean ± SEM. Statistical analysis was done by paired t-tests. *P < 0.05, **P < 0.01, ***P < 0.001, ****P < 0.0001 and not significant (ns) P > 0.05. **a**,**i** were created with BioRender.com

Figure 4: ΔHER2^{CD5} enhances the safety of CAR T cells as safety switch

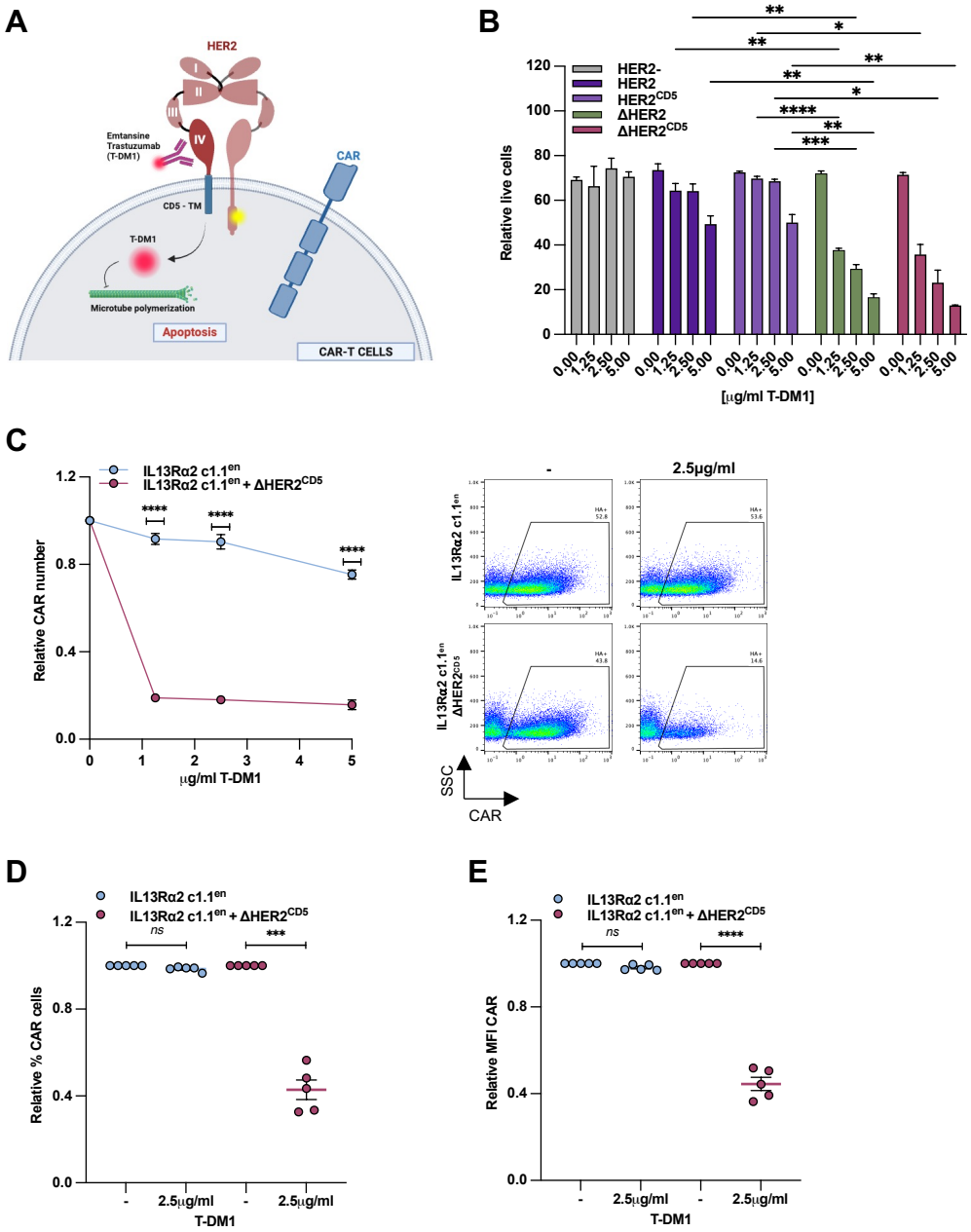

Figure 4: ΔHER2^{CD5} enhances the safety of CAR T cells as safety switch

A. Schematic representation of the HER2 mode of action as suicide switch created with BioRender.com. **B.** Relative percentage of live (DAPI^{-} Annexin-V^{-}) Jurkat cells overexpressing full length HER2, HER2 with CD5 transmembrane or truncated HER2 following T-DM1 exposure at the indicated concentrations for 72h. Results are expressed as a representative of three independent experiments. **C.** IL13Rα2 c1.1^{en} and IL13Rα2 c1.1^{en} +ΔHER2^{CD5} CAR-T cell number following 48h treatment with the indicated concentration of T-DM1 (n=6). Positive CAR-T expressing cells were counted using Precision Count Beads. A representative flow cytometry plot is shown on the right. Percentage (**D**) and MFI (**E**) of IL13Rα2 c1.1^{en} and IL13Rα2 c1.1^{en} +ΔHER2^{CD5} CAR-T cell following treatment with 2.5μg/ml of T-DM1. Cohorts are shown as mean ± SEM. Statistical analysis was done by paired t-tests. *P < 0.05, **P < 0.01, ***P < 0.001, ****P < 0.0001 and not significant (ns) P > 0.05.

Figure 5: IL13Rα2 c1.1^{en} Arm CAR shows resistance to TGF-β and enhanced cell persistence *in vitro* and *in vivo*

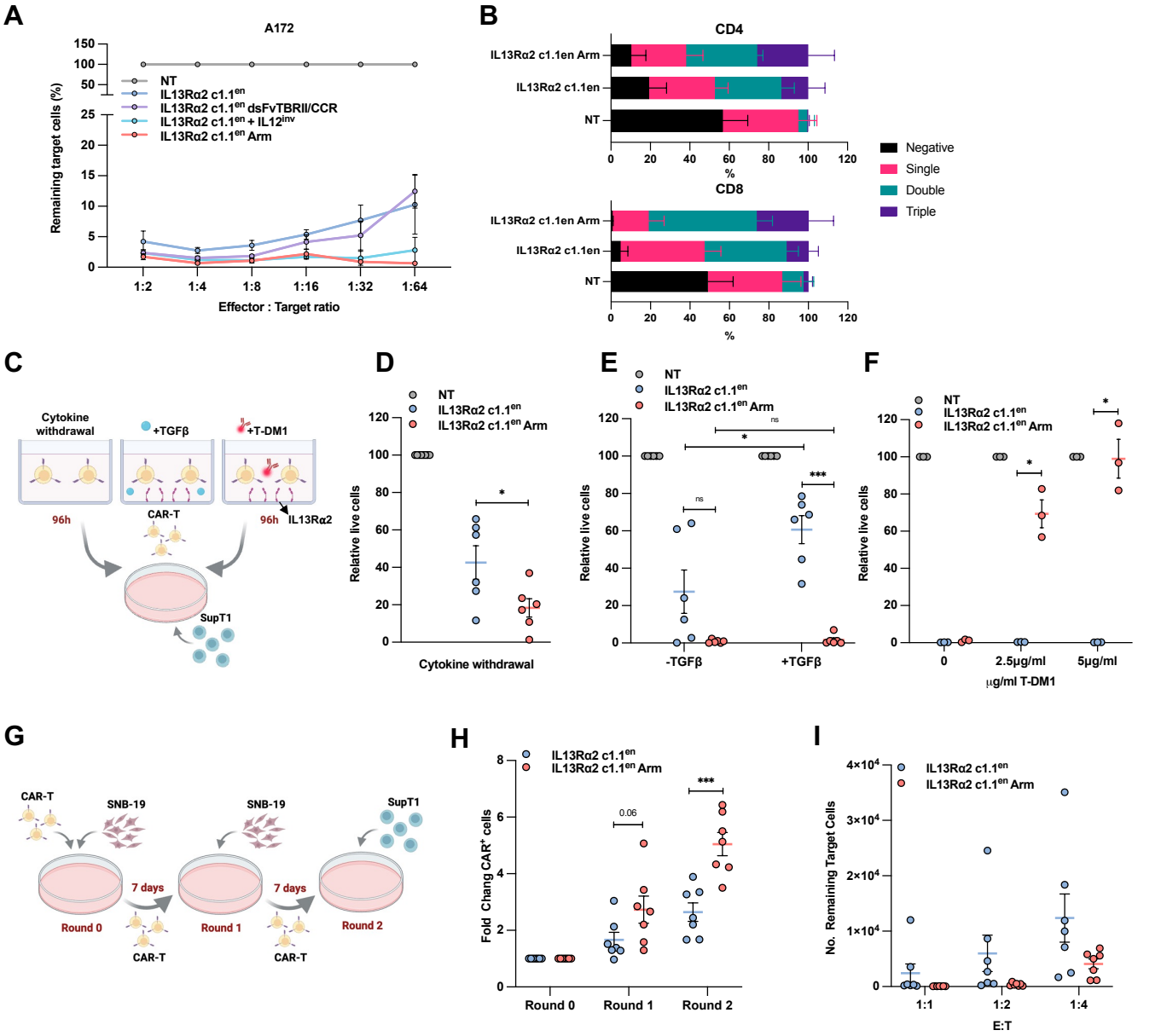

Figure 5: IL13Rα2 c1.1^{en} Arm CAR shows resistance to TGFβ1 and enhanced cell persistence in vitro

A. Viable target A172 cells following co-culture with IL13Rα2 c1.1^{en} or IL13Rα2 c1.1^{en} Arm CAR-T cells and single armoured CAR-T cells at the indicated E:T ratio quantified by flow cytometry. The percentage of live target cells was calculated by normalizing to the NT group. **B.** Co-expression of TIM3, LAG3 and PD-1 on IL13Rα2 c1.1^{en} and IL13Rα2 c1.1^{en} Arm CAR T cells within CD4^{+} and CD8^{+} subsets after 3-day co-culture with IL13Rα2-expressing targets. **C.** Schematic representation of the experimental layout. In brief, CAR-T cells were cultured in a cytokine-deprived medium or in the presence of 1ug/ml IL13Rα2 immobilised protein with or without TGFβ1 or T-DM1 for 96h. A fixed volume of cells was then transferred to a plate containing SupT1-IL13Rα2 to measure their cytotoxic activity. Following another 96h, viable target cells were quantified by flow cytometry (**D**,**E**,**F**). **G.** Schematic representation of the experimental layout. In brief, CAR-T cells were co-cultured with SNB19 for 7 days (round 0) before being counted and re-seeded on fresh SNB19 for an extra 7 days (round 1). The cells were then counted, normalised and cultivated with SupT1-IL13Rα2 target cells for 48 hours (round 2). The fold increase of CAR-positive cells after each round of replating is shown in (**H**). The cytotoxic activity at the indicated E:T ratio following re-plating after round 1 is shown in (**I**). Cohorts are shown as mean ± SEM. Statistical analysis was done by paired t-tests. *P < 0.05, **P < 0.01, ***P < 0.001, ****P < 0.0001 and not significant (ns) P > 0.05. **C**,**G** were created using BioRender.com

Figure 6: IL13Rα2 c1.1^{en} Arm CAR shows enhanced cell persistence *in vivo*

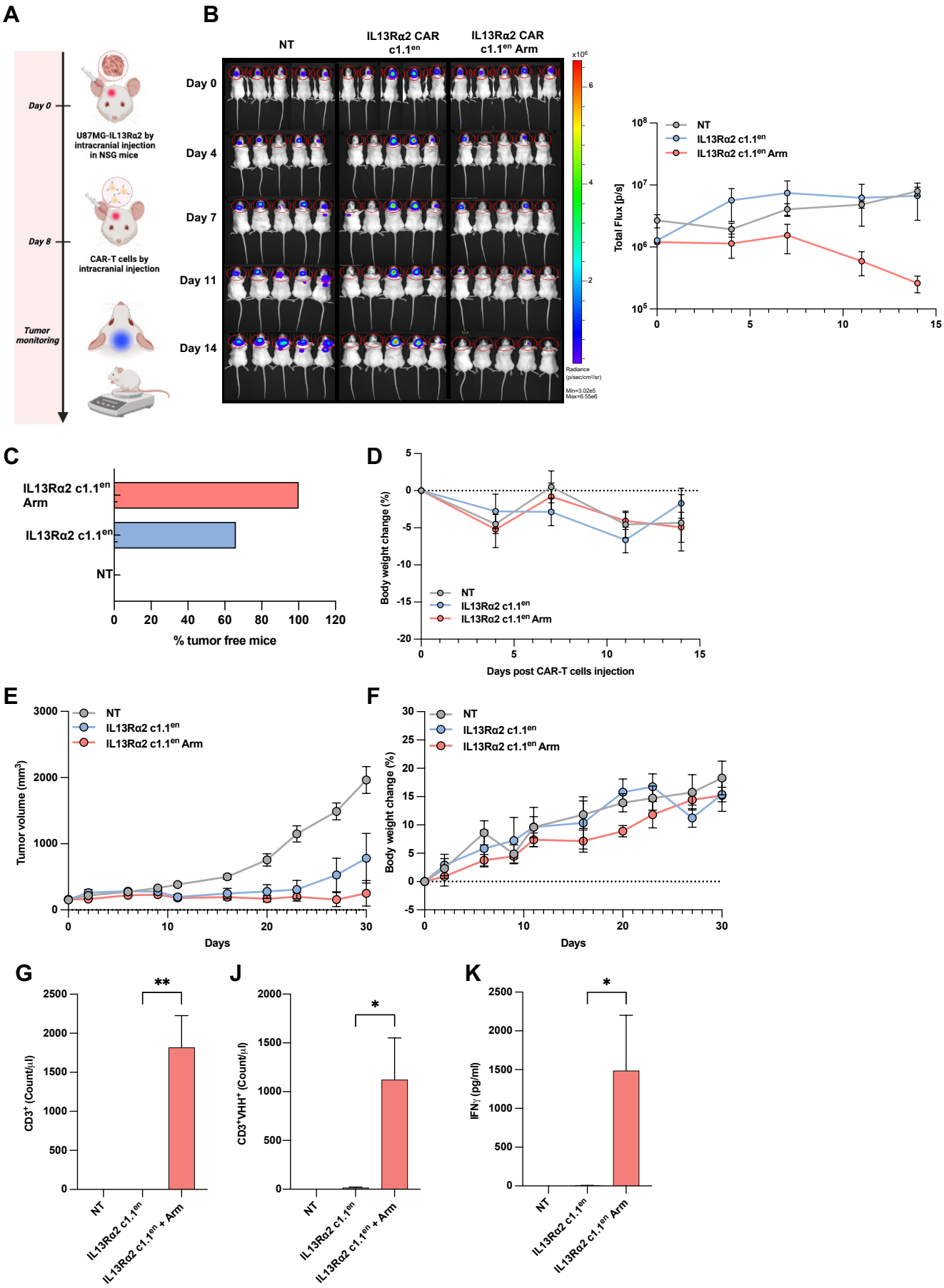

Figure 6: IL13Rα2 c1.1^{en} Arm CAR shows enhanced cell persistence in vivo

A. Design of the orthotopic in vivo experiment. (created using BioRender.com) **B.** Bioluminescence (BLI) images and values at day 0, 4, 7, 11 and 14 after untransduced (NT), IL13Rα2 c1.1^{en} or IL13Rα2 c1.1^{en} Arm CAR-T cells injection. **C.** Bars represent the percentage of tumor-free mice at day 14. **D.** Body weight at day 0, 4, 7, 11 and 14 after untransduced (NT), IL13Rα2 c1.1^{en} or IL13Rα2 c1.1^{en} Arm CAR-T cells injection. Tumor volume (**G**) and body weight (**H**) measurements of NSG mice subcutaneously injected with U87-IL13Rα2 target cells, which were allowed to engraft for 8 days before a 5x10^{6} dose of non-transduced T or CAR-T cells was intravenously injected via the tail vein. **I,J.** Number of hCD3^{+} and HA^{+} cells quantified by FACS analysis at sacrifice (day 30). **K.** Quantification of IFN-γ levels in plasma samples collected from mice at day 30 post-treatment. IFN-γ concentrations were measured by ELISA.

Cohorts are shown as mean ± SEM. Statistical analysis was done by paired t-tests. *$P < 0.05$, **$P < 0.01$, ***$P < 0.001$, ****$P < 0.0001$ and not significant (ns) $P > 0.05$.

Figure 7: Validation of the IL13Rα2 c1.1^{en}multi-armoured CAR (NS007) for clinical use

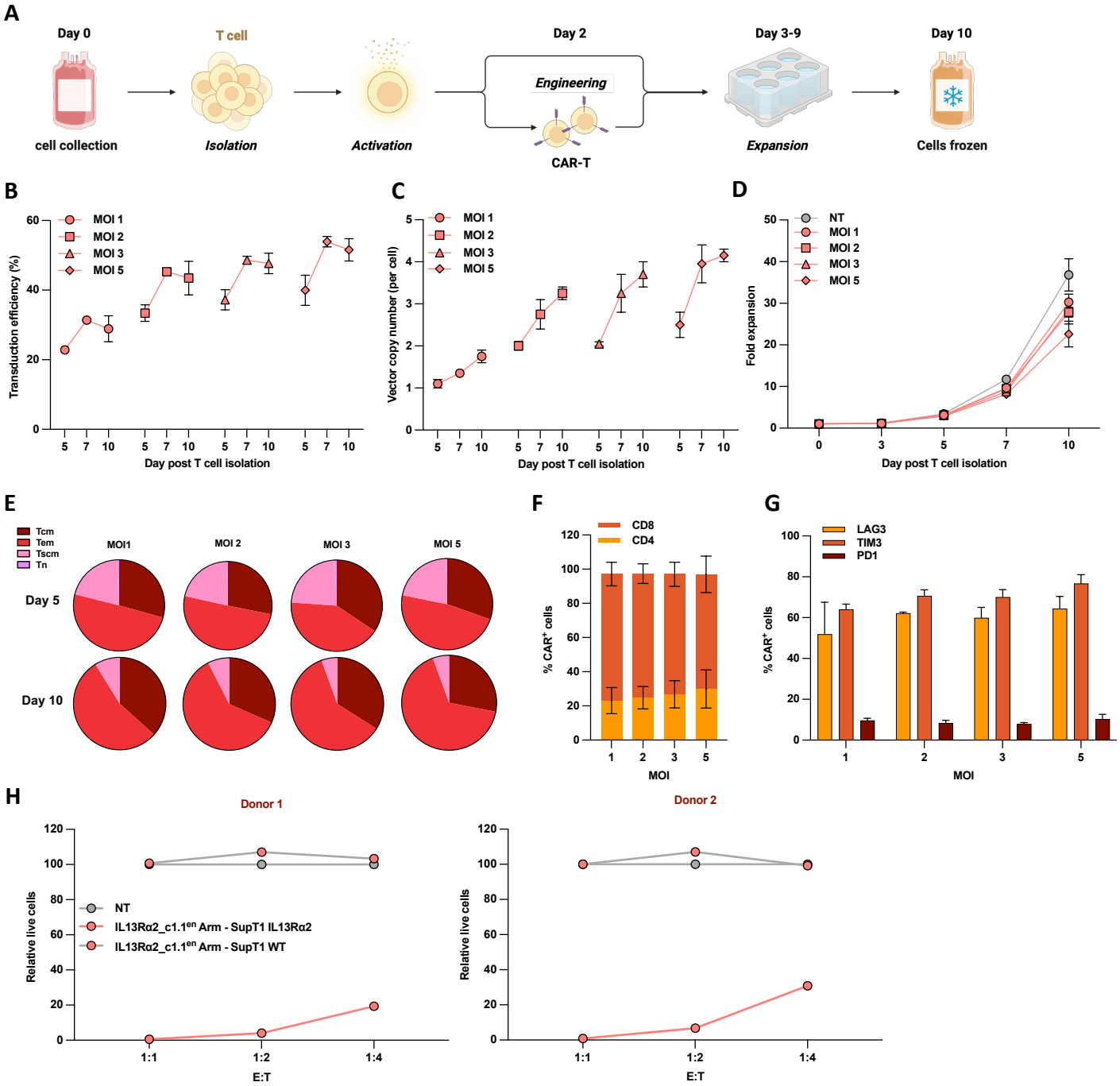

Figure 7: Validation of the IL13Rα2 c1.1^{en}multi-armoured CAR (NS007) for clinical use

A. Schematic representation of the manufacturing protocol created with biorender.com. Transduction efficiency (**B**) and vector copy number (VCN) (**C**) at day 5, 7 and 10 post T cell isolation at the indicated multiplicity of infection (MOI). **D.** Fold change in T cell expansion over a period of 10 days**. E.** Naïve (Tn), central memory (Tcm), effector memory (Tem) and memory stem cells (Tscm) T-cell subsets were identified following gating on CD45RA and CCR7 expression. Ratio of CD4:CD8 (**F**) and expression of exhaustion markers (**G**) in CAR-T positive cells 10 days post T cell isolation. **H**. Viable target SupT1-IL13Rα2 and SupT1 cells following co-culture with GMP grade manufactured IL13Rα2 c1.1en Arm CAR-T cells at the indicated E:T ratio quantified by flow cytometry. The percentage of live target cells was calculated by normalizing to the NT group. Cohorts are shown as mean ± SD of two independent healthy donors.

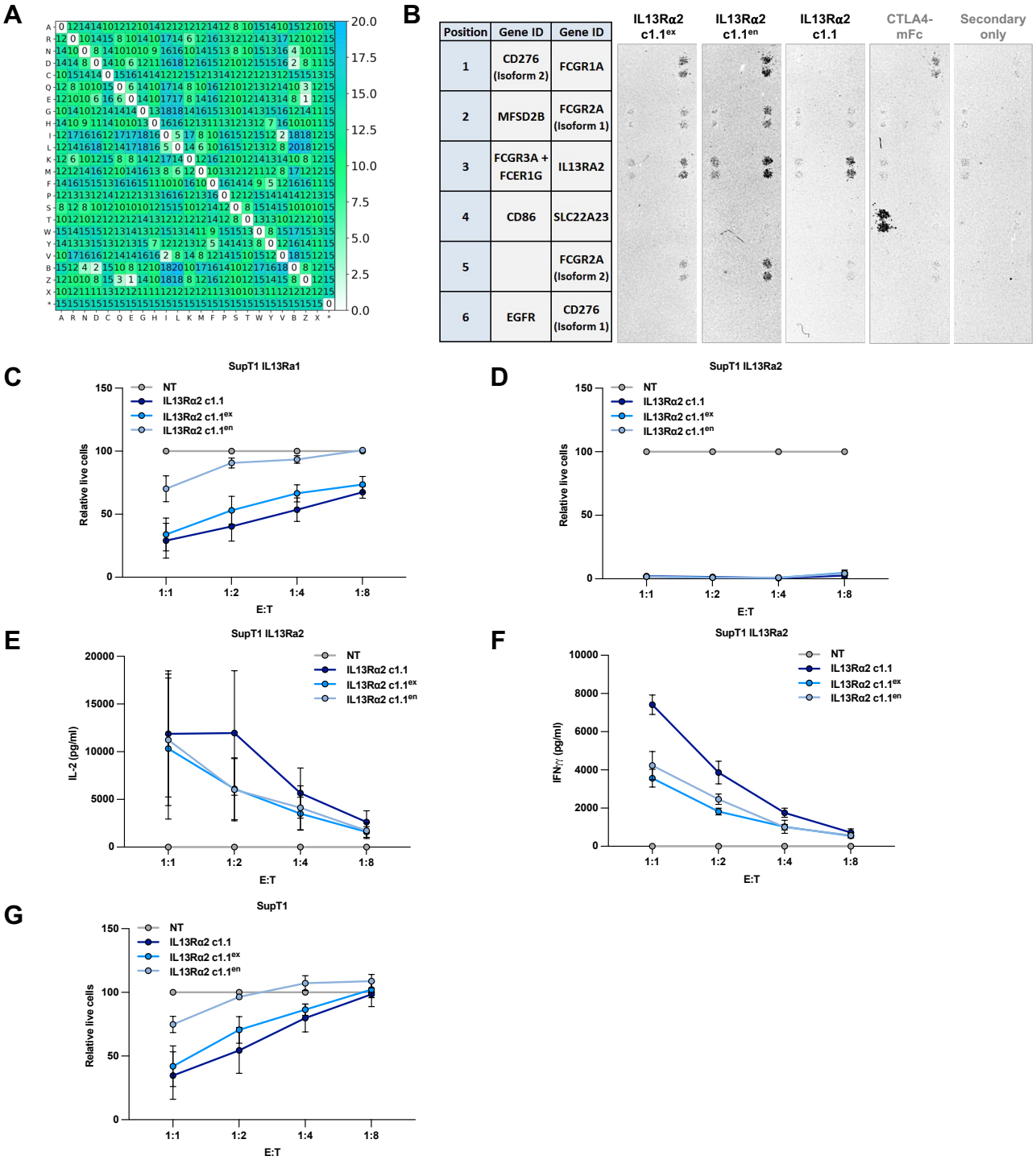

Supplementary Figure S1: *In vitro* screening identifies lead IL13Rα2 VHH for CAR-T cells.

A. Distribution matrix depicting chemical distances between amino acids based on substitution scores. **B.** The IL13Rα2 c1.1, IL13Rα2 c1.1ex, and IL13Rα2 c1.1en VHHs were Fc-conjugated and used to stain an array containing ~6000 native human membrane proteins. Binding to Fc gamma receptors (e.g., FcGR1A and FcGR2A isoforms) is expected due to the Fc conjugation. The figure shows representative intensity of the staining against selected proteins. Each column corresponds to a different VHH construct, with two dots per protein indicating duplicate spots on the array for technical validation. **C,D.** SupT1 expressing IL13Rα1 (**C**) or IL13Rα2 (**D**) were co-cultured with different ratios of CAR-T cells for 72 hours. Viable target cells were quantified by flow cytometry using CD2 and CD3 expression as exclusion markers. The percentage of live target cells was calculated by normalizing to the NT group. **E,F.** ELISA detection of IL-2 and IFN-γ production by CAR-T cells co-cultured with SupT1-IL13Rα2 cells at the indicated E:T ratio (relative to Figure 1h). **G**. Quantification of live SupT1 cells following co-culture with CAR-T cells at the indicated E:T ratio for 72h.

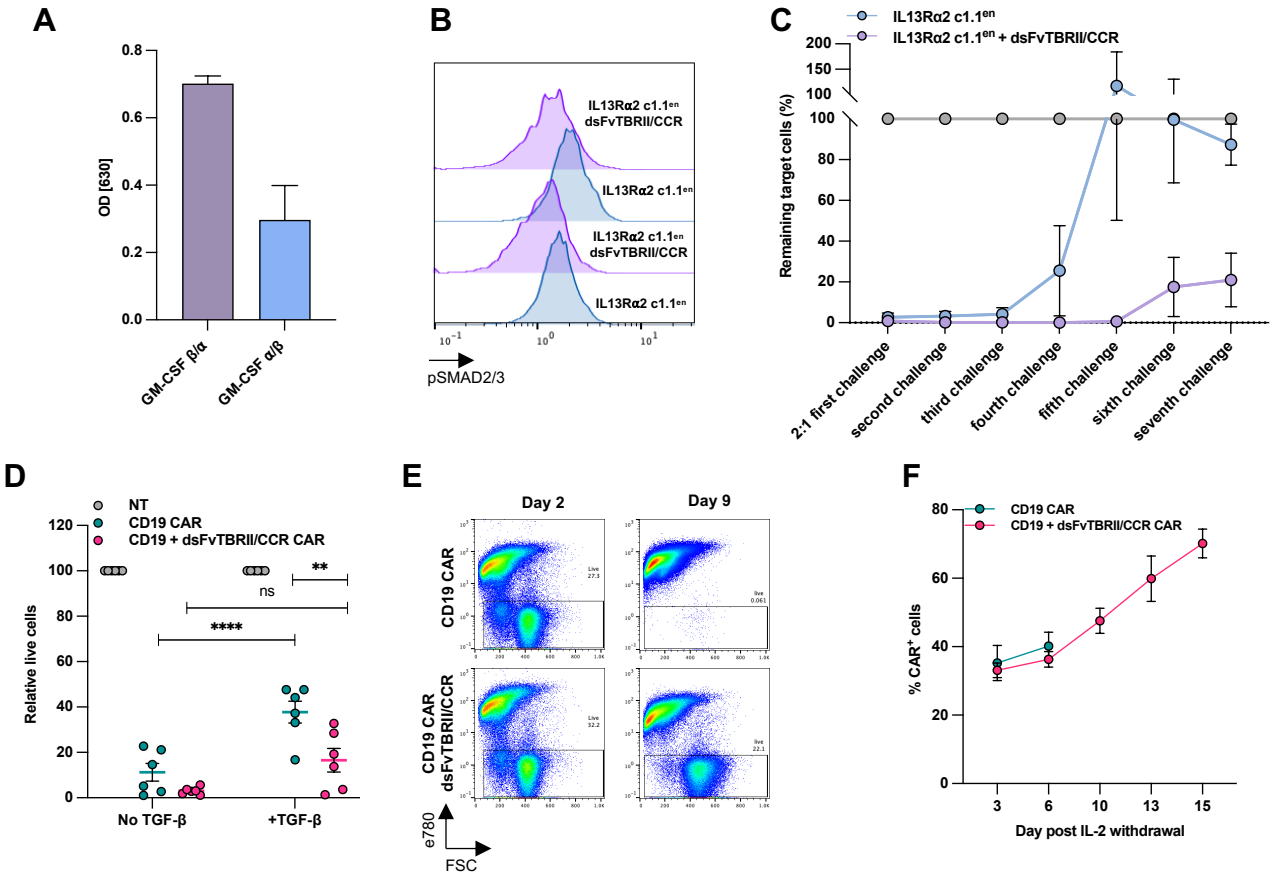

Supplementary Figure S2: dsFvTBRII/CCR overcomes the inhibitory effects of TGF-β and induces CAR-T cell persistence.

A. Quantification of the SEAP secreted by HEK-Blue™ TGF-β expressing the dsFvTBRII region fused with different orientations of the GM-CSF receptor chains: alpha-beta and beta-alpha. **B.** Representative FACS histograms of pSMAD2/3 expression following TGFβ stimulation (related to Figure 2E). **C.** T cells expressing IL13Rα2 c1.1^{en} CAR or IL13Rα2 c1.1^{en} CAR+dsFvTBRII/CCR were harvested and co-cultured with fresh SNB19 once a week for 7 weeks. Remaining SNB19 cells were quantified using precision counting beads via FACS. **D**. SupT1 expressing CD19 were co-cultured with different ratios of CAR-T cells for 72h with or without 10ng/ml TGFβ. Then, viable target cells were quantified by flow cytometry using CD2 and CD3 expression, and the percentage of live target cells was calculated by normalizing to the NT group. **E.** Representative flow cytometry plot from an individual T cell donor expressing CD19 CAR or CD19 CAR+dsFvTBRII/CCR following cytokine withdrawal at the indicated time point. A total of three independent experiments were conducted, each using lymphocytes from a different healthy donor. **F.** Analysis of CAR-positive cell enrichment over time following cytokine withdrawal measured by flow cytometry (n=3). Cohorts are shown as mean ± SEM. Statistical analysis was done by paired t-tests. *$P < 0.05$, **$P < 0.01$, ***$P < 0.001$, ****$P < 0.0001$ and not significant (ns) $P > 0.05$.

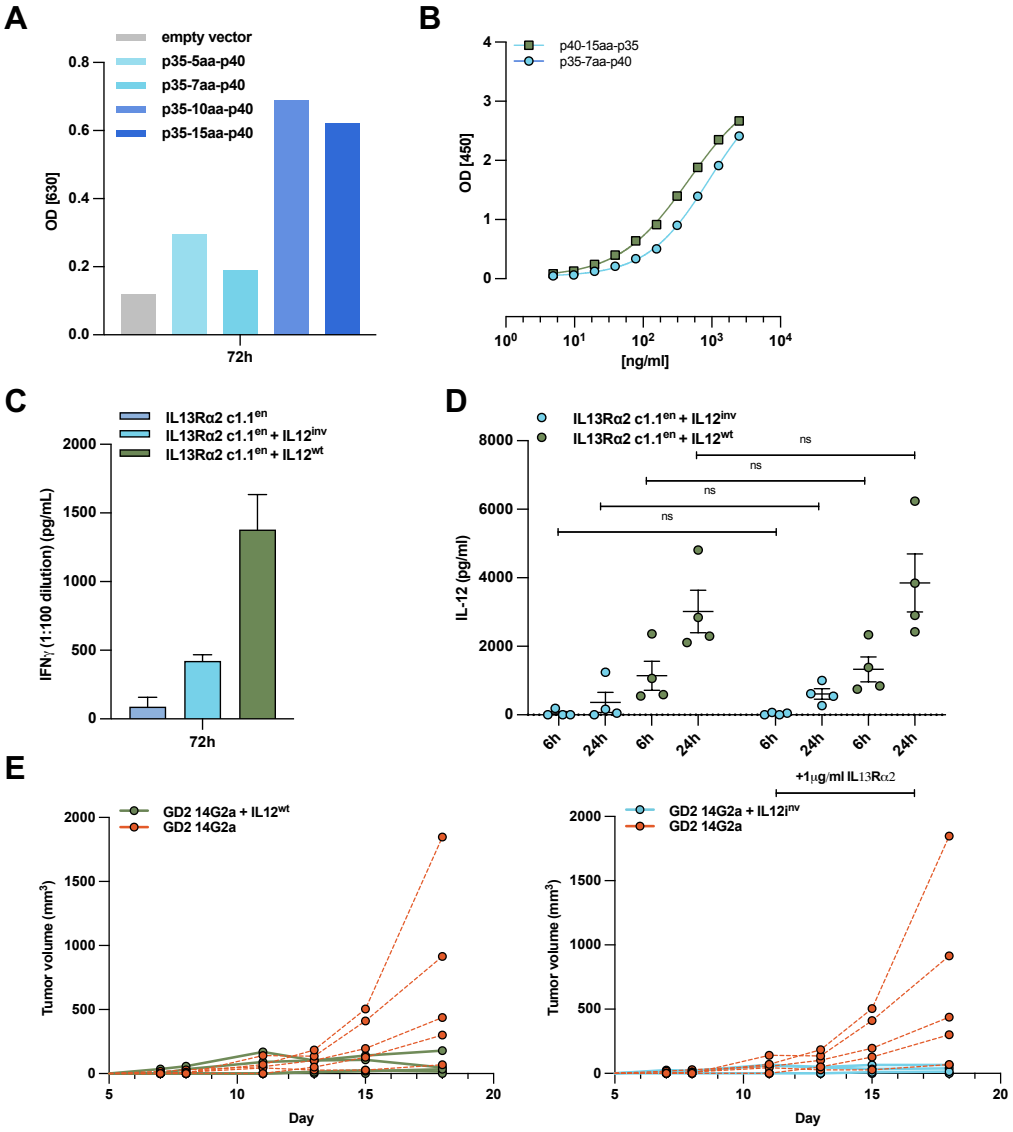

Supplementary Figure S3: scIL12^{inv} demonstrates enhanced safety while preserving its potent anti-cancer effects

A. Quantification of the SEAP secreted by HEK-Blue™ IL12 cultured in the presence of Jurkat cells expressing the p35 subunit followed by the p40 and connected with the indicated linker lengths for 72h. Results are expressed as representative of three independent experiments. **B.** Affinity of the designed p40-15aa-p35 and p35-7aa-p40 scIL12s to the immobilised IL12β2 was evaluated by ELISA assay (related to Figure 3c). **C.** ELISA detection of IFNγ production by NK cells co-cultured with Jurkat cells expressing IL13Rα2 c1.1^{en}, IL13Rα2 c1.1^{en}+IL12^{wt} or IL13Rα2 c1.1^{en}+IL12^{inv} CAR for 72h (related to Figure **3G**). Cohorts are shown as mean ± SEM **D.** ELISA detection of IL12 production quantified by p70 analysis following IL13Rα2 stimulation of IL13Rα2 c1.1^{en}+IL12^{wt} or IL13Rα2 c1.1^{en}+IL12^{inv} CAR-T cells for the indicated time. **E.** Tumour volume measurement of each mouse used in the B16.F10-GD2 *in vivo* study (related to Figure **3J**).

*P < 0.05, **P < 0.01, ***P < 0.001, ****P < 0.0001 and not significant (ns) P > 0.05.

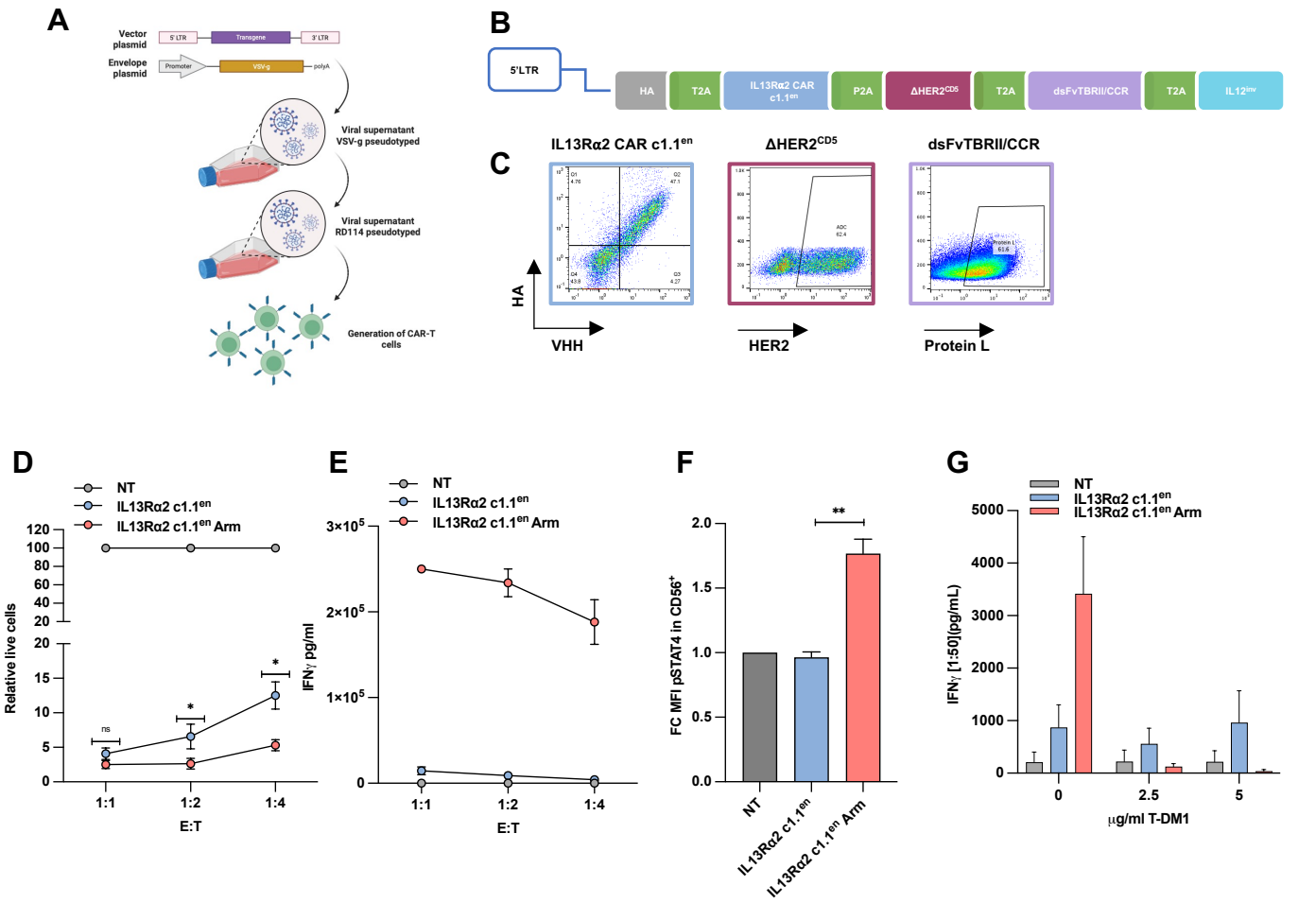

Supplementary Figure S4: IL13Rα2 c1.1^{en} Arm CAR shows resistance to TGF-β and enhanced cell persistence *in vitro* and *in vivo*

A. Schematic showing CAR vector with armouring modules. The vectors include an N-terminal transduction marker (HA) followed by the IL13Rα2 c1.1^{en}. The additional armoured modules were inserted in the indicated order and separated by self-cleaving 2A peptides. LTR, long terminal repeat. **B.** Representative flow cytometry plots showing the detection of the IL13Rα2 c1.1^{en} CAR and armoured modules. Results are expressed as representative of three independent donors for lymphocytes. **C.** Schematic representation of the transduction protocol created with Biorender.com. **D.** Viable target SNB19 cells following co-culture with IL13Rα2 c1.1^{en} or IL13Rα2 c1.1^{en} Arm CAR-T cells at the indicated E:T ratio quantified by flow cytometry. The percentage of live target cells was calculated by normalizing to the NT group. **E.** Quantification of IFN-γ production of CAR-T cells co-cultured with SNB19 target cells (related to Figure **5C**). **F.** pSTAT4 level in CD56^{+} cells following co-culture with CAR-T cells expressing IL13Rα2 c1.1^{en} or IL13Rα2 c1.1^{en} Arm for 72h. **G.** ELISA detection of IFNγ production of CAR-T cells co-cultured with SupT1-IL13Rα2 target cells following pre-exposure to T-DM1 at the indicated concentration (related to Figure **5F**).

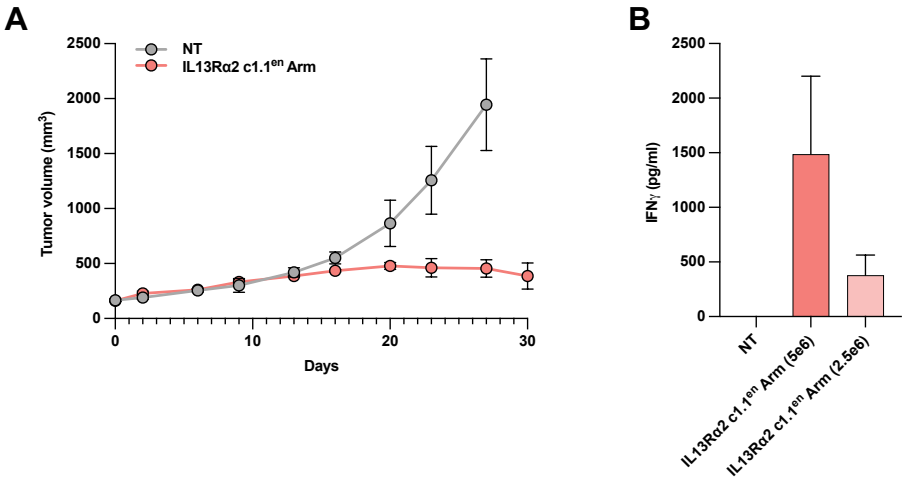

Supplementary Figure S5: IL13Rα2 c1.1^{en} Arm CAR shows enhanced cell persistence *in vivo*

A. Tumor volume measurements of NSG mice subcutaneously injected with U87-IL13Rα2 target cells, which were allowed to engraft for 8 days before a 2.5x10^6 dose of non-transduced T or CAR-T cells was intravenously injected via the tail vein. **B.** Quantification of IFN-γ levels in plasma samples collected from mice at day 30 post-treatment. IFN-γ concentrations were measured by ELISA.